LAMINAR FILMWISE CONDENSATION OF FLOWING VAPOR ON A SPHERE

A THESIS SUBMITTED TO
THE GRADUATE SCHOOL OF NATURAL AND APPLIED SCIENCES
OF
MIDDLE EAST TECHNICAL UNIVERSITY

BY

DOĞUŞ EROL

IN PARTIAL FULFILLMENT OF THE REQUIREMENTS FOR THE DEGREE OF
MASTER OF SCIENCE
IN
MECHANICAL ENGINEERING

JUNE 2004

Approval of the Graduate School of Natural and Applied Sciences

_____

Prof. Dr. Canan ÖZGEN
Director

I certify that this thesis satisifies all the requirements as a thesis for the degree of Master of Science.

_____

Prof. Dr. S.Kemal İDER
Head of Department

This is to certify that we have read this thesis and that in our opinion it is fully adequate,in scope and quality,as a thesis for the degree of Master of Science

_____

Assoc. Prof. Dr. Cemil YAMALI
Supervisor

Examining Committee Members

Prof. Dr. Faruk ARINÇ (Chairman) _____

Assoc. Prof. Dr. Cemil YAMALI (Supervisor) _____

Prof. Dr. Kahraman ALBAYRAK _____

Asst. Prof. Dr. İlker TARI _____

Prof. Dr. Ali DURMAZ (Gazi Univ.) _____

I hereby declare that all information in this document has been obtained and presented in accordance with academic rules and ethical conduct. I also declare that, as required by these rules and conduct, I have fully cited and referenced all material and results that are not original to this work.

Name, Last name :

Signature :

ABSTRACT

LAMINAR FILMWISE CONDENSATION OF FLOWING VAPOR ON A SPHERE

EROL, Doğuş
M.S., Department of Mechanical Engineering
Supervisor:Assoc. Prof. Dr.Cemil YAMALI

June 2004 , 81 pages

The objective of this study is to analyze theoretically the laminar film condensation of water vapor flowing on a sphere. For this purpose, the problem was handled by including all of the two-phase boundary layer parameters such as gravity, effect of vapor shear, inertia, energy convection and pressure gradient. For this full two-phase boundary layer system, the boundary layer equations, boundary conditions and the interfacial conditions were first analyzed, and then discretized. A computer program in Mathcad, solving these discretized equations, was written to obtain the velocity and temperature profiles within the condensate, the velocity profiles within the vapor, the condensate film thickness and the local Nusselt number. The

effects of pressure gradient, gravity, vapor oncoming velocity and sphere radius on these parameters were examined. By alternating the formulation of the problem, the results for the flow over a horizontal cylinder were obtained. These results were then compared with those for the sphere. Finally, the results for the system with Mercury vapor flowing on a sphere were obtained. All of these results were represented as diagrams and tables, and were discussed at the end of the study.

Keywords: Laminar, film condensation, interfacial shear, horizontal cylinder, sphere, discretization

ÖZ

KÜRE ÜZERİNDE AKAN BUHARIN LAMİNER FİLM ŞEKLİNDEKİ YOĞUŞMASI

EROL , Doğuş
Y.Lisans, Makine Mühendisliği Bölümü
Tez Yöneticisi: Doç. Dr.Cemil YAMALI

Haziran 2004 , 81 sayfa

Bu projenin amacı, su buharının küre üzerinde laminer yoğuşmasının teorik olarak incelenmesidir. Bu amaçla, problem iki fazlı sınır film ile ilgili olan yer çekimi, buharın uyguladığı kesme gerilimi, atalet kuvvetleri, taşınım ısı transferi ve basınç gradyanı gibi parametreler ele alınarak çözülmüştür. Bu komple iki fazlı sınır film ile ilgili ilk olarak sınır film denklemleri, sınır şartları ve arayüzey şartları analiz edilmiş, ve daha sonra da bunlar diskretize edilmiştir. Sıvı içindeki hız ve sıcaklık profillerini, buharın hız profilini, sıvı film kalınlığını ve yerel Nusselt sayısını hesaplamak amacıyla MathCad'de, bu diskretize edilmiş denklemleri çözen bir program geliştirilmiştir. Ayrıca, basınç gradyanı, yerçekimi, buhar akış hızı ve küre çapının yukarıda belirtilen parametrelere etkisi araştırılmıştır. Problemin formulasyonu değiştirilerek

yatay silindir üzerinden akış için sonuçlar elde edilmiştir. Daha sonra bunlar küre için elde edilen sonuçlar ile karşılaştırılmıştır. Son olarak küre üzerinde cıva buharının aktığı sistem için sonuçlar elde edilmiştir. Bütün sonuçlar grafik ve tablolar ile gösterilmiş ve çalışmanın sonunda yorumlanmıştır.

Anahtar kelimeler: Laminer, film yoğuşması, arayüzey kesme gerilmesi, yatay silindir, küre, diskretizasyon

ACKNOWLEGEMENTS

I would like to thank my supervisor, Assoc .Prof. Dr. Cemil YAMALI for his continuous guidance, support and valuable contribution throughout this study.

I offer sincere appreciation to my family and my fiancée for their help and endurance to me, understanding and support.

TABLE OF CONTENTS

LIST OF TABLES

TABLE

LIST OF FIGURES

FIGURE

LIST OF SYMBOLS

C_p	Average heat capacity, W/K
g	Gravitational acceleration, m/s^2
h_{fg}	Latent heat, J/kg
k_l	Thermal conductivity of liquid, W/mK
k_v	Thermal conductivity of vapor, W/mK
T_s	Saturation temperature, K
T_w	Wall temperature, K
p	Pressure, N/m
r_o	Sphere radius, m
r	Distance from the axis of symetry, m
ϕ	Angle from the upper stagnation point, deg.
U_∞	Oncoming flow speed, m/s
U_v	Potential flow velocity, m/s
u_l	x component of condensate velocity, m/s
v_l	y component of condensate velocity, m/s
u_v	x component of vapor velocity, m/s
v_v	y component of vapor velocity, m/s
x	Coordinate parallel to surface, m
y	Coordinate normal to surface, m
Δx	Increment in x-direction, m

Δy	Increment in x-direction, m
α_l	Thermal diffusivity of condensate, m^2/s
α_v	Thermal diffusivity of vapor, m^2/s
Δ	Thickness of vapor boundary layer, m
δ	Thickness of condensate layer, m
η	Dimensionless coordinate (y/δ)
$\Delta\eta$	Increment in x-direction
μ_l	Dynamic viscosity of condensate, kg/ms
μ_v	Dynamic viscosity of vapor, kg/ms
ν_l	Kinematic viscosity of condensate, m^2/s
ν_v	Kinematic viscosity of vapor, m^2/s
ρ_l	Density of condensate, kg/m^3
ρ_v	Density of vapor, kg/m^3
τ_i	Shear stress at liquid-vapor interface, N/m^2
h	Heat transfer coefficient, W/m^2K
Nu	Local Nusselt number
m	Mesh point coordinate in x-direction
n	Mesh point coordinate in η-direction
k	Mesh point coordinate in y-direction
N	The last mesh point within the condensate
K	The last mesh point within the vapor

CHAPTER 1

INTRODUCTION

1.1. Condensation

Condensation is defined as the phase change from the vapor state to the liquid state, and occurs when the temperature of the vapor is reduced below its saturation temperature. This is usually done by bringing the vapor into contact with a solid surface whose temperature is below the saturation temperature of the vapor. But condensation can also occur on the free surface of a liquid or even in a gas when the temperature of the liquid or the gas, to which the vapor is exposed, is below the saturation temperature. In the latter case, the liquid droplets suspended in the gas form a fog.

Two distinct forms of surface condensation are observed: film condensation and dropwise condensation.

1.1.1. Film Condensation

Film condensation is the most widely observed mode, and takes place if the liquid wets the condenser surface, resulting in the coverage of the surface by a liquid condensate film of increasing thickness. This liquid film between solid surface and the vapor serves as a resistance to heat transfer,

and is removed from the surface under the action of body forces and/or shear stresses due to vapor flow. The first analytical formulation was carried out by Nusselt. In this analysis gravity and viscous forces were considered and a linear temperature profile within the condensate layer was assumed.

1.1.2. Dropwise Condensation

Dropwise condensation occurs if the condensate does not wet the condenser surface. In this type of condensation vapor in contact with a subcooled surface form microscopic droplets on the surface, which then grow by the direct condensation on the droplets and by coalescences between the droplets, until a certain size is reached. There is no liquid film in this case to resist heat transfer. As a result, heat transfer rates that are more than 10 times larger than those associated with film condensation can be achieved with dropwise condensation. Therefore, dropwise condensation is the preferred mode of condensation in heat transfer. However, it is very difficult to obtain dropwise condensation, since it doesn't last long and converts to film condensation after some time. Therefore, it is more realistic to assume film condensation in the design of heat transfer equipment.

1.2. The Presence of Noncondensable Gases in Vapor

Most condensers used in steam power plants operate at pressures well below the atmospheric pressure (usually under 0.1 atm), and operation at such low pressures raises the possibility of air (a noncondensable gas) leaking into the condensers. Experimental studies show that even small amounts of a noncondensable gas in the vapor cause significant drops in heat transfer coefficient during condensation. The drastic reduction in the condensation heat transfer coefficient can be explained as follows: When the

vapor mixed with a noncondensable gas condenses, only the noncondensible gas remains in the vicinity of the surface. This gas layer acts as a barrier between the vapor and the surface, and makes it difficult for the vapor to reach the surface. The vapor now must diffuse through the noncondensable gas before reaching the condensate surface, and this reduces the effectiveness of the condensation process.

Experimental studies show that a high flow velocity improves the condensation heat transfer, since it is more likely to remove the stagnant noncondensable gas from the vicinity of the condensate surface [1].

1.3. Viscous Fluid Flow

1.3.1. Boundary Layer

At a stationary surface over which a viscous fluid flows, the fluid particles adhere to the surface and the frictional forces between the fluid layers retard the motion of the fluid within a thin layer near the surface. In this thin layer, which is called the boundary layer, the velocity of the fluid decreases from its freestream value to a value of zero at the surface (no-slip condition).

Ludwig Prandtl introduced the boundary layer concept for the first time in 1904. According to Prandtl's boundary layer concept, under certain conditions viscous forces are of importance only in the immediate vicinity of a solid surface (in the boundary layer) where the velocity gradients normal to the surface are large. In regions removed from the solid surface where there exists no large gradients in fluid velocity, the fluid motion may be considered frictionless, i.e., potential flow.

There is, in fact, no precise dividing line between the potential flow region, where friction is negligible, and the boundary layer region. However, it is customary to define the boundary layer as that region where the velocity component parallel to the surface is less than 99% of the freestream velocity. Since the velocity component parallel to the surface is varying, the continuity requires that there should also be a velocity component perpendicular to the surface [2].

1.3.2. Laminar and Turbulent Flow

In the treatment of any flow problem, one should first determine whether the flow is laminar or turbulent. Surface friction and convection heat transfer rates strongly depend on which of these conditions exist.

In the laminar flow, fluid motion is ordered and it is possible to identify streamlines along which particles the fluid move. The flow is steady and two dimensional. The velocity component perpendicular to the surface contributes significantly to the transfer of momentum and energy through the flow layers.

Fluid motion in the turbulent flow is highly irregular and is characterized by disorderly displacements of individual volumes of fluid within the flow. These displacements enhance the transfer of momentum and energy. Velocity, temperature, pressure and other properties change continuously in time, and the flow is unsteady and three-dimensional. The structure of turbulence is a complex phenomena which is still not fully understood, and semi-empirical methods are invariably used for the solution of engineering problems.

If the flow over a flat plate is considered, initially the boundary layer development is laminar, but at some critical distance from the leading edge

small disturbances in the flow begin to and a transition process takes place until the flow in the boundary layer becomes fully turbulent [3].

1.3.3. Flow Separation

For flow separation, there must be a driving force to slow down the wall flow and can make it go backward. This driving force is termed the adverse pressure gradient. The flow over a flat plate is a boundary layer flow without pressure gradient and hence, there is no flow separation. But, for boundary layer flows such as the flow over a cylinder or sphere, there begins an adverse pressure gradient after some location in the flow, and the increasing downstream pressure causes the wall flow to separate [4,5].

CHAPTER 2

REVIEW OF PREVIOUS STUDIES

The present work concerns the numerical analysis of laminar film condensation of vertically flowing vapor on a sphere. Film condensation of vapor has been the subject of a large number of theoretical and experimental works since the early studies of Nusselt.

Sparrow and Gregg [6] revealed the role of inertia forces and energy convection for gravity induced condensate flow along a vertical plate. They used a similarity transformation to obtain ordinary differential equations from the partial differential equations of the boundary layer and then solved these equations. In the analysis, invoking an overall energy balance it was shown that the liquid film thickness increases monotonically with the subcooling parameter $C_p\Delta T/h_{fg.}$ Heat transfer results were obtained for values of the parameter $C_p\Delta T/h_{fg}$ between 0 and 2 for Prandtl numbers between 0.003 and 100. The authors showed that the effect of the inertia forces on heat transfer is negligible for $Pr \geq 1$, but becomes important when $Pr \ll 1$ for a constant value of the subcooling parameter $C_p\Delta T/h_{fg}$ (or liquid film thickness). They also showed that the effect of inertia forces becomes also more important when the parameter $C_p\Delta T/h_{fg}$ increases. In the study, energy convection was found to play a minor role for $Pr \ll 1$, and to increase with film thickness for $Pr \geq 1$.

In a later study of Sparrow and Gregg [7] a similar boundary layer analysis including the effects of inertia and energy convection was made for laminar film condensation on a horizontal cylinder. The problem for the cylinder was modeled in cartesian coordinates. The authors found a similarity solution which is valid for the cylinder surface except the stagnation region where the boundary layer assumptions are already invalid. Similar to the vertical plate case, they found that for high Prandtl number fluids the effects of energy convection become more important, and the heat transfer increases with increasing film thickness. However, for low Prandtl number fluids, where the heat conductivity overrides the energy convection, the effects of the inertia forces became more important, and the heat transfer decreased with increasing film thickness. In the study, the film thickness was found to grow rather slowly over the upper portion of the cylinder and then to grow rapidly over the lower portion until it becomes infinity at the lower stagnation point.

Yang [8] made a boundary layer analysis for laminar film condensation on a sphere. Assuming stagnant vapor and zero shear at the edge of the condensate layer, similarity transformations of the axi-symmetrical boundary layer equations were made in the analysis for two cases. The first case included both the inertia forces and energy convection, and was valid for the upper stagnation region. The second case excluded the inertia forces, and was valid for the entire surface of the sphere. Results for heat transfer, film thickness and condensation rate were obtained for four Prandtl numbers: 100, 10, 1 and 0.03 in the range of the subcooling term, $C_p\Delta T/h_{fg}$, from 0.001 to 1. For the same subcooling term, the heat transfer rate was found to increase with Prandtl number, and for the same Prandtl number, to decrease with the increase of subcooling. The effects of Prandtl number and subcooling on film thickness and on condensation rate were found to be the opposite to that on heat transfer. On the other hand, the condensation rate increased with the subcooling parameter. For Pr=0.03, including the inertia of the condensate yielded a thicker film and reduced the heat transfer. For $Pr \geq 1$

heat transfer rate, film thickness and condensation rate were not affected by the inertia forces. At the end of the study, the author found a correlation for the average Nusselt number for the entire sphere surface to compare it with that of a vertical plate and a horizontal cylinder found by Sparrow and Gregg [6,7]. For a given Prandtl number and subcooling, he found that the average Nusselt number of a sphere of diameter D was 8.8% higher than that of a horizontal cylinder of the same diameter, and was 17.6% lower than that of a vertical plate of height D.

The boundary layer approach including the shear force at the liquid-vapor interface was first studied by Koh, Sparrow and Hartnett [9] for laminar film condensation of stationary vapor along a vertical plate. The authors put forward the idea that the interfacial shear causes the liquid to induce vapor velocities and hence reduce the heat transfer. Thus, they solved the two-phase boundary layer equations including the inertia forces and energy convection for the problem considered. The inclusion of the shear force at the liquid surface was handled by applying a force balance at the interface. In the analysis, similarity transformation was used and it was found that the effect of interfacial shear on heat transfer is negligible small for $Pr \geq 1$. But, for liquid metals, the interfacial shear was shown to cause a significant reduction in heat transfer. It was also shown that increasing the thickness of the condensate film causes the interfacial shear and inertia forces to be more effective in reducing heat transfer for all Prandtl numbers. The effect of the parameter $(\rho\mu)_l/(\rho\mu)_v$, arising from the shear force balance at the liquid-vapour interface, on heat transfer was found to be negligible small.

The effect of interfacial shear at the liquid-vapor interface was later analyzed by Chen [10] by applying an modified integral method for laminar film condensation along a vertical plate. It was assumed that the ratio $(\rho\mu)_v/(\rho\mu)_l$ is negligible small, and the vapor drag at the edge of the liquid film is approximately equal to the momentum of entering vapor. Similar to the study of Koh, Sparrow and Hartnett [9], as a result of the vapor drag, the

author found lower heat transfer rates (especially at low Prandtl numbers) compared with Sparrow and Gregg [6]. He also showed that a significant negative velocity gradient at the interface occurs except for small acceleration parameter $k\Delta T/\mu_l h_{fg}$.

In a later study of Chen [11], the effect of interfacial shear at the liquid-vapor interface was studied for the case of laminar film condensation on a horizontal cylinder. With the assumptions made for the vertical plate case the modified integral method was applied to the cylinder. Velocity and temperature profiles were obtained for the case of $(\rho\mu)_v/(\rho\mu)_l<<1$, and similarity was found to exist exactly near the top stagnation point and approximately for the most part of the tube. Compared with the vertical plate case, this analysis has shown that the inertia forces, which are stronger for the top half of the cylinder, have a larger effect on heat transfer except for values of $k\Delta T/\mu_l h_{fg}<0.5$.

Koh [12] solved the two-phase boundary layer equations of laminar film condensation along a vertical plate by applying an integral method. In the analysis inertia forces, energy convection and interfacial shear were included as done by references [8,9,10]. It was shown analytically why the parameter $(\rho\mu)_l/(\rho\mu)_v$ does not play a significant role and hence only two parameters, $C_p\Delta T/h_{fg}$ and Pr are involved in film condensation problem. The subcooling parameter $C_p\Delta T/h_{fg}$ was found to increase the heat transfer for Pr>1, and to decrease the heat transfer for Pr<1. The calculated heat transfer results and velocity profiles agree well with the results from the exact solution of the boundary layer equations carried out by Koh, Sparrow and Hartnett [8] (max. deviation of 5 %).

An approximate similarity solution of the model of Koh, Sparrow and Hartnett [9] was carried out by Churchill [13]. Solutions were presented for the effects of inertia and heat capacity of the condensate and interfacial shear. The effects of inertia of the condensate and interfacial shear on heat

transfer were both found to be appreciable for Pr<5. As noted by the previous authors, the heat capacity of the condensate was shown to increase the rate of heat transfer for Pr>1 and has the opposite effect for Pr<1. In the study, also the effect of of surface curvature on laminar film condensation outside and inside vertical tubes was investigated. It was found that this effect increases the heat transfer significantly for condensation outside the tube only for Nusselt numbers less than 26, and decreases the heat transfer inside the tube correspondingly.

The effect of surface curvature for laminar film condensation on a horizontal cylinder was studied by Taghavi [14]. In the analysis, he assumed that inertia forces and energy convection are negligible small and the shear at the condensate surface is zero. To show the effect of surface curvature, first the momentum equation was solved in cylindrical coordinates. Then, the results were written in terms of the solution for the case of negligible curvature effect, i.e., solution for the momentum equation written in cartesian coordinates. It was found that for the range of ordinary Nusselt numbers, the assumption of negligible surface curvature effect is reasonable (deviation<1%).

Henderson and Marchello [15] studied the role of surface tension and tube diameter on film condensation of stationary vapour on horizontal tubes. They used the data of various observers to get a set of the $h_{measured}$ / $h_{Nusselt}$ ratio. Once the set was obtained, they used least squares fit and found a correlation for the h_m / h_{Nu} ratio which contains the corrections due to the effects of surface tension and pipe diameter, which are important at the bottom of the tube. The correlation they obtained contained the Ohnesorge number which is expressed as $\mu/(\rho g D \sigma)^{1/2}$.

For the first time, in a study of Koh [16], laminar film condensation in forced flow was analyzed along a horizontal plate. In the study inertia and gravity forces were neglected and energy convection was included. The

analysis was done by solving the ordinary differential equations obtained by similarity transformation of the partial differential two-phase boundary layer equations. The interfacial shear was included by writing a force balance at the vapor-liquid interface as done by Koh, Sparrow and Hartnett [9]. The results were presented as a function of $C_p\Delta T/h_{fg}$ with $(\rho\mu)_l/(\rho\mu)_v$ and Prandtl number as parameters. For low Prandtl number liquids, the author found that energy transfer by convection is negligible small and the heat transfer decreases monotonically as the parameter $C_p\Delta T/h_{fg}$ increases. For high Prandtl number liquids, it was found that energy convection plays an important role and the heat transfer drops to a minimum value and then rises again as the condensate film thickness increases.

Shekriladze and Gomelauri [17] studied laminar film condensation of flowing vapor along a horizontal plate and over a horizontal cylinder. In their study; pressure gradient, inertia and gravity forces, energy convection and condensate subcooling were neglected. The vapor drag was assumed to arise mainly from the momentum transferred due to the vapor suction as done in the studies of Chen and Churchill [10,11,13]. For the flat plate case, correlations for the effects of inertia forces and energy convection were found. These effects on heat transfer were found to be negligible small for ordinary liquids. For the horizontal cylinder case, the authors first found a relation for the mean heat transfer coefficient. Then, they modified this relation according to the fact that 65% of heat is transferred up to the minimum separation angle of 82°. For condensation in a gravitational field they stated that an explicit analytical solution is impossible.

Denny and Mills [18] analyzed laminar film condensation of flowing vapor on a horizontal cylinder including the gravity forces which have been neglected by Shekriladze and Gomelauri [17]. The authors developed an analytical solution for the problem neglecting inertia forces, energy convection and pressure gradient around the cylinder. The accuracy of this solution was compared with exact numerical solutions also done in this study.

The results of their analysis showed that negligible inertia assumption is violated as ϕ (angle measured from the vertical axis) becomes higher then 140°. But the results were assumed to be important since in a typical situation 85% of total condensation takes place when $\phi < 140°$ and surface tension effects near the bottom of the tube cannot be ignored. In the analysis it was also shown that the pressure gradient leads to an increase in overall heat transfer coefficient, and its effect on local heat transfer coefficient decreases as ϕ increases.

The effect of vapor velocity on laminar film condensation of flowing vapor on a horizontal cylinder was studied by Fujii, Uehara and Kurata [19]. In their study gravity forces, inertia forces for the vapor boundary layer, energy convection and pressure gradient were all included. The problem of the interfacial shear was dealed with the model of Koh, Sparrow and Hartnett [8]. A similarity solution was obtained assuming potential flow outside the vapor boundary layer and making use of power series expansion. A simple expression for the average and local heat transfer coefficient was obtained. Also experiments for condensation of steam were performed in the study. Comparing the theoretical results with experimental ones, the authors concluded that, for high oncoming velocities, the effect of body forces on heat transfer is negligible small and the $\rho\mu$ ratio is important. The authors also concluded that the local heat transfer coefficients at the upper part of the tube become higher with increasing oncoming velocity.

Rose [20] analyzed the effect of pressure gradient for forced convection film condensation on a horizontal cylinder. The inertia forces were neglected and the simpler Shekriladze and Gomelauri model for the vapor drag was adopted since the primary object was to investigate the effect of pressure gradient in the analysis. Potential flow outside the vapor boundary layer was assumed. The analysis concluded that the pressure gradient becomes important when the parameter $\rho gd / 8\rho_g U_\infty^2$ becomes smaller than unity. Furthermore, the pressure gradient was shown to lead to higher heat

transfer coefficients for the upper part of the cylinder and to cause instability in the condensate film at some location over the rear half.

Approximations such as zero gravity, negligible inertia, negligible energy convection etc. May be justified in many cases, but they cannot be generalized over the whole range of the governing parameters. Thus, Gaddis [21] solved the full two-phase boundary layer equations for laminar film condensation of flowing vapor on a horizontal cylinder by transforming the governing partial differential equations into ordinary differential equations. He showed that for quiescent vapor (Re=0) and for liquid metals, ignoring inertia forces in the condensate film and shear forces at the interface leads to an important increase in heat transfer, whereas subcooling in the condensate is ineffective. But, for ordinary liquids, ignoring inertia forces in the condensate film and shear forces at the interface were shown to have insignificant effect on heat transfer, whereas liquid subcooling caused a reduction of 5% in heat transfer. For flowing vapor ($Re \neq 0$), the author showed that increasing Reynolds number leads to an increase in heat transfer, as long as flow separation does not occur. At the end of his study, it was shown that for $Re=10^5$, the flow separates from the wall at $\phi=126°$.

Karabulut and Ataer [22] carried out a numerical analysis of laminar film condensation of vapor flowing downwards a horizontal cylinder, including the inertia forces, pressure gradient and energy convection in the two-phase boundary layer equations. Instead of transforming the basic equations into a set of ordinary differential equations as done by Gaddis [20], they applied a direct numerical method to the basic equations. They first discretized the basic equations of the boundary layer, and then solved the discretized equations numerically. For steam with a freestream velocity of 20 m/s, and with a temperature difference of 10 °C, they found that flow separation takes place at $\phi=108°$. The comparison of the condensate thickness with and without the pressure gradient term has showed that the pressure gradient makes the condensate flow unstable over the lower part of the cylinder. But,

the effect of pressure gradient on heat transfer was found to be insignificant. The effect of the flow velocity was shown to decrease the condensate film thickness and hence, to increase the heat transfer from the interface to the wall. In the study, errors due to the omission of inertia forces and energy convection were also examined and found to be insignificant except at high oncoming velocity and ΔT.

Memory, Adams and Marto [23] studied laminar film condensation on horizontal elliptical tubes under the condition of free and forced convection. The effect of surface tension was included in the analysis. For free convection, the shear force at condensate film edge was assumed to be zero. For forced convection, interfacial shear and pressure gradient around the tube were included. The results for free convection showed that an elliptical tube with major axis vertically placed leads to an improvement of 11% in mean heat transfer coefficient compared to a circular tube of equivalent surface area. For the case of forced convection at a given oncoming velocity, 2% decrease in the mean heat transfer coefficient was observed due to a reduction in interfacial shear. However, for the same pressure drop across each tube, heat transfer was 16% higher for the elliptical tube. The surface tension effect on mean heat transfer coefficient was found to be negligible small.

.

CHAPTER 3

ANALYSIS

3.1. Description of the Model

The physical model is shown in orthogonal curvilinear coordinates in Figure 3.1. The arc length x is measured along the surface of the sphere and has a initial value of zero at the upper stagnation point. The normal distance y is measured from the surface of the sphere. It is assumed that the sphere is situated in a large body of pure vapor at saturated state flowing vertically with temperature T_s and oncoming velocity U_∞. The saturated vapor condenses on the surface of the sphere, which is at a uniform temperature T_w ($T_w<T_s$). The removal of the condansate is induced by gravity and interfacial shear caused by the vapor. At some location ϕ, the flow separates from the wall, and the boundary layer theory is not valid anymore. Outside the vapor boundary layer, the flow is ideal. The undisturbed vapor velocity and the force of gravity have the same direction.

For the system under consideration, the equivalent model in cartesian coordinates is shown in Figure 3.2.

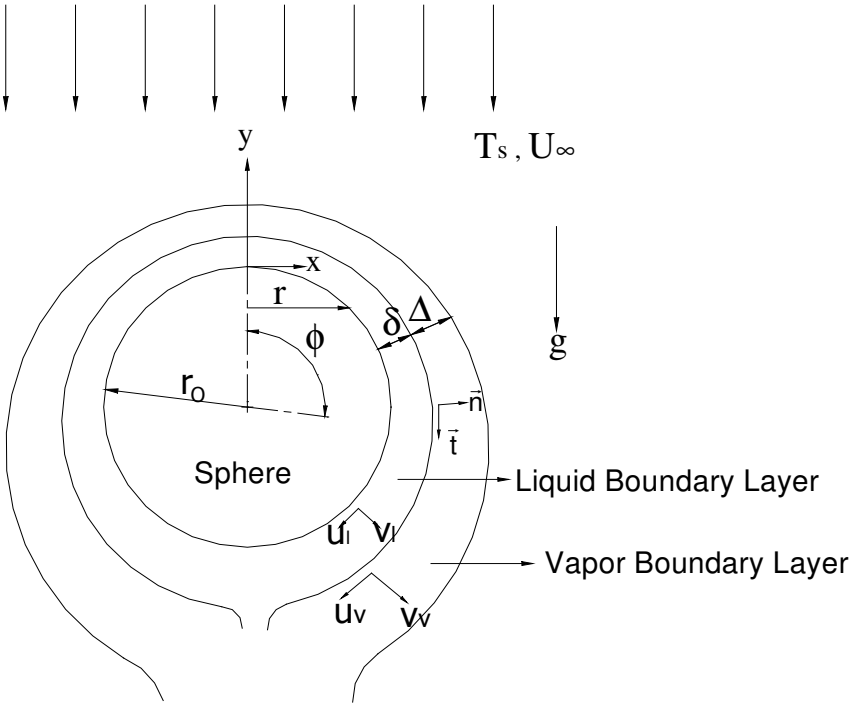

Figure 3.1. Physical Model

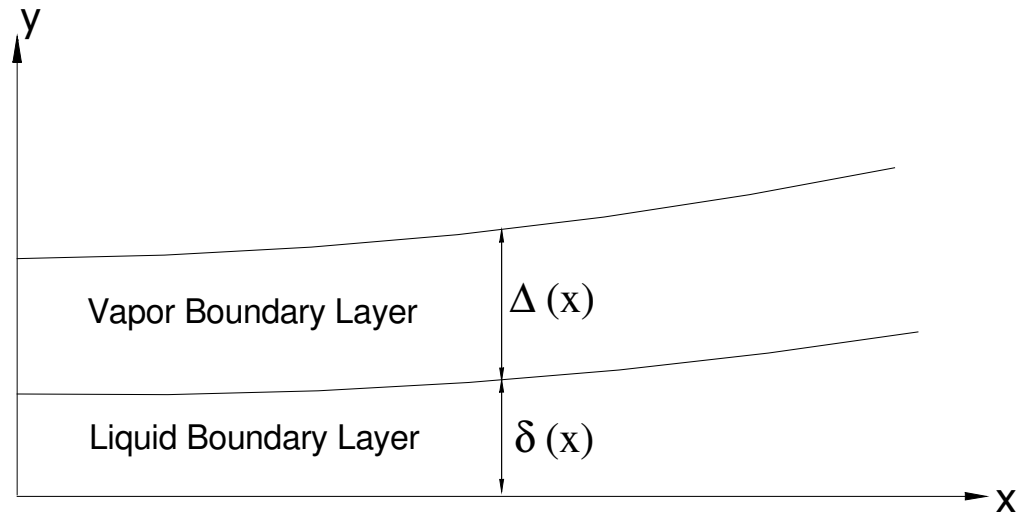

Figure 3.2. Equivalent Model in Cartesian Coordinates

3.2. Assumptions

In the formulation of the problem the following assumptions have been made:

(1) The flow in the condensate film and vapor boundary layer are laminar up to the separation point.
(2) The flow over the sphere is axially symetrical.
(3) All physical properties are constant.
(4) Thicknesses of the condensate film (δ) and vapor boundary layer (Δ) are very small compared with sphere radius (r_o).
(5) The vapor is pure, dry and saturated.
(6) Steady state is achieved.
(7) Surface tension forces are insignificant.
(8) Temperature variations at liquid-vapor interface between the liquid and vapor phases are insignificant.
(9) Undisturbed vapor velocity is steady and uniform.
(10) Surface temperature is uniform.
(11) Viscous dissipation is ignored.
(12) Outside the vapor boundary layer, there is potential flow.

3.3. Boundary Layer Equations

3.3.1. For the Liquid Boundary Layer

Conservation of Mass Equation [8]:

$$\frac{\partial}{\partial x}(r u_l) + r\frac{\partial}{\partial y}(v_l) = 0 \qquad (3.1)$$

where;

$$r = r_0 \sin\frac{x}{r_0} \qquad (3.2)$$

Conservation of Momentum Equation [22]:

$$u_l \frac{\partial u_l}{\partial x} + v_l \frac{\partial u_l}{\partial y} = -\frac{1}{\rho_l}\frac{dp}{dx} + \upsilon_l \frac{\partial^2 u_l}{\partial y^2} + g\sin\phi \tag{3.3}$$

Since $x \cong \phi r_o$, this equation can be rewritten as;

$$u_l \frac{\partial u_l}{\partial x} + v_l \frac{\partial u_l}{\partial y} = -\frac{1}{\rho_l}\frac{dp}{dx} + \upsilon_l \frac{\partial^2 u_l}{\partial y^2} + g\sin\left(\frac{x}{r_o}\right) \tag{3.4}$$

Conservation of Energy Equation [22]:

$$u_l \frac{\partial T}{\partial x} + v_l \frac{\partial T}{\partial y} = \alpha_l \frac{\partial^2 T}{\partial y^2} \tag{3.5}$$

3.3.2. For the Vapor Boundary Layer [4]

Conservation of Mass Equation:

$$\frac{\partial}{\partial x}(r u_v) + r\frac{\partial}{\partial y}(v_v) = 0 \tag{3.6}$$

where;

$$r = r_0 \sin\frac{x}{r_0} \tag{3.7}$$

Conservation of Momentum Equation:

$$u_v \frac{\partial u_v}{\partial x} + v_v \frac{\partial u_v}{\partial y} = -\frac{1}{\rho_v}\frac{dp}{dx} + \upsilon_v \frac{\partial^2 u_v}{\partial y^2} \tag{3.8}$$

For the vapor boundary layer, the saturation condition implies that the vapor temperature is constant. Consequently, the conservation of energy equation need not to be considered.

3.4. Boundary and Interfacial Conditions

3.4.1. Boundary Conditions

At x = 0:

$$u_l = 0 \tag{3.9}$$

$$u_v = 0 \tag{3.10}$$

$$\frac{\partial T}{\partial x} = 0 \tag{3.11}$$

$$\frac{d\delta}{dx} = 0 \tag{3.12}$$

At y = 0 (liquid-solid interface):

$$u_l = 0 \tag{3.13}$$

$$v_l = 0 \tag{3.14}$$

$$T = T_w \tag{3.15}$$

At $y = \delta + \Delta$ (vapor boundary layer edge):

At the edge of the vapor boundary layer, the velocity component in x-direction approaches the velocity in the main stream asymptotically. Since outside the vapor boundary layer ideal flow is assumed, the main stream

velocity is obtained from the ideal flow theory [24].

$$U_v = \frac{3}{2} U_\infty \sin\left(\frac{x}{r_o}\right) \tag{3.16}$$

The pressure gradient in the liquid layer and vapor boundary layer is also obtained from the ideal flow theory.

$$-\frac{1}{\rho_v}\frac{dp}{dx} = U_v \frac{dU_v}{dx} \tag{3.17}$$

3.4.2. Interfacial Conditions

The velocity, mass transfer and shear force along the liquid-vapor interface must be matched in both liquid and vapor phases in such a way that the physical laws are satisfied. These matching conditions are explained in more detail in Ref.[9].

a) Interface Velocity:

Along the liquid-vapor interface, the velocities tangent to the interface must be equal if there is no slip;

$$(u_t)_l = (u_t)_v \tag{3.18}$$

The normal and tangent unit vectors respectively at the interface are:

$$\vec{n} = \frac{\vec{j}\, dx - \vec{i}\, d\delta}{\sqrt{dx^2 + d\delta^2}} \tag{3.19}$$

$$\vec{t} = \frac{\vec{i}\, dx + \vec{j}\, d\delta}{\sqrt{dx^2 + d\delta^2}} \tag{3.20}$$

The velocity at the interface is:

$$\vec{u} = \vec{i}\,u - \vec{j}\,v \tag{3.21}$$

Hence, the velocity tangent to the interface is:

$$u_t = \vec{u}\cdot\vec{t} = \frac{u\,dx - v\,d\delta}{\sqrt{dx^2 + d\delta^2}} \tag{3.22}$$

Consequently, under the assumptions of boundary layer theory, the no slip condition, expressed as Eq.(3.18), at the interface is fulfilled if the velocity components in x-direction are equal;

$$u_l = u_v \tag{3.23}$$

b) Interface Shear Stress:

According to Newton's Third Law the shear stress at the interface for Newtonian fluids can be expressed as;

$$\vec{\tau} = \vec{i}\,\mu\left(\frac{\partial u}{\partial y} + \frac{\partial v}{\partial x}\right) + \vec{j}\,\mu\left(\frac{\partial u}{\partial y} + \frac{\partial v}{\partial x}\right) \tag{3.24}$$

So, the shear stress tangent to the interface becomes:

$$\tau_i = \vec{\tau}\cdot\vec{t} = \frac{\mu dx\left(\frac{\partial u}{\partial y} + \frac{\partial v}{\partial x}\right) + \mu d\delta\left(\frac{\partial u}{\partial y} + \frac{\partial v}{\partial x}\right)}{\sqrt{dx^2 + d\delta^2}} \tag{3.25}$$

Hence, under the assumptions of boundary layer theory, the tangential shear balance at the interface requires the following condition:

$$\tau_i = \mu_l \frac{\partial u_l}{\partial y} = \mu_v \frac{\partial u_v}{\partial y} \tag{3.26}$$

c) Interface Mass Flow:

The mass transfer per unit area across the interface can be expressed as:

$$\rho v_n = \rho(\vec{u}\cdot\vec{n}) = \frac{\rho v dx - \rho u d\delta}{\sqrt{dx^2 + d\delta^2}} \tag{3.27}$$

Therefore, under the assumptions of boundary layer theory, mass conservation at the interface requires the following condition [9,22]:

$$\rho_v\left(u_v \frac{d\delta}{dx} - v_v\right) = \frac{k_l}{h_{fg}}\left(\frac{dT}{dy}\right)_{y=0} \tag{3.28}$$

d) Interface Temperature:

Saturated vapor is assumed to flow around the sphere. Hence, the temperature at the interface is:

$$T = T_s = \text{constant} \tag{3.29}$$

3.5. The Overall Energy Balance

From an energy balance in the condensate layer [8];

$$\int_0^{\delta} h_{fg}\,\rho_l\,u_l\,2\pi r\,dy = \int_0^{x} k_l\left(\frac{\partial T}{\partial y}\right)_{y=0} 2\pi r\,dx \tag{3.30}$$

The left hand side of this equation is the latent heat of condensation. The right hand side is the heat transferred from the condensate to the wall over a length from x=0 to x=x. Eq. (3.30) can be rewritten as;

$$\frac{\partial}{\partial x} r \int_0^{\delta} u_l \, dy = \frac{k_l}{h_{fg} \rho_l} r \left(\frac{\partial T}{\partial y} \right)_{y=0} \tag{3.31}$$

Since $r = r(x)$, if the above equation is rearranged;

$$\int_0^{\delta} \frac{\partial}{\partial x} (r u_l) dy = \frac{k_l}{h_{fg} \rho_l} r \left(\frac{\partial T}{\partial y} \right)_{y=0} \tag{3.32}$$

3.6. Normalization of the Solution Domain in the Liquid Film

By introducing $\eta = y/\delta$, the solution domain in the condensate is normalized and the model is shown in Fig.3.3.

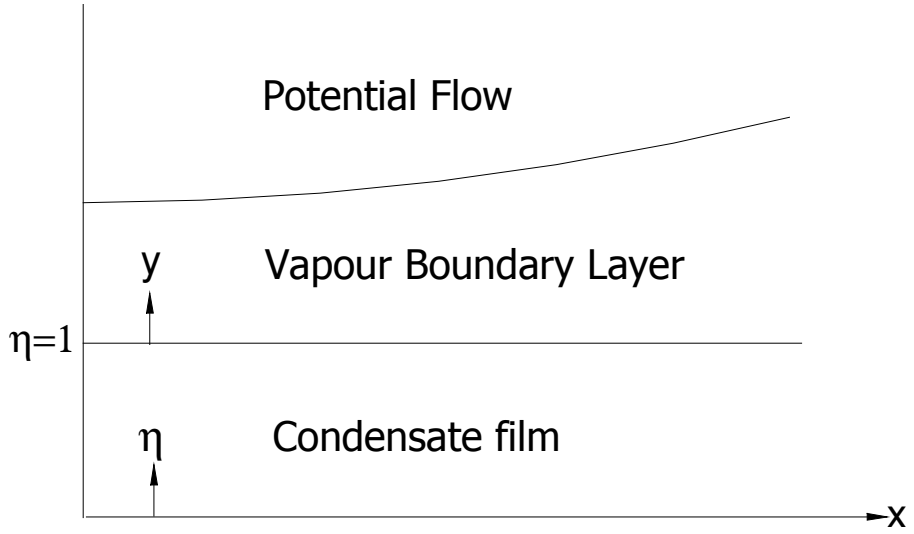

Figure 3.3. Normalization of the Solution Domain in the Condensate

The boundary layer equations for the liquid film; Eq.(3.1), (3.4) and (3.5) can be rewritten as (also Eq.(3.17) is substituted into Eq.(3.4));

$$\frac{\partial}{\partial x} (r u_l) + \frac{r}{\delta} \frac{\partial}{\partial \eta} (v_l) = 0 \tag{3.33}$$

$$u_l \frac{\partial u_l}{\partial x} + \frac{v_l}{\delta} \frac{\partial u_l}{\partial \eta} = \frac{\rho_v}{\rho_l} U_v \frac{dU_v}{dx} + \frac{\upsilon_l}{\delta^2} \frac{\partial^2 u_l}{\partial \eta^2} + g \sin\left(\frac{x}{r_o}\right) \tag{3.34}$$

$$u_l \frac{\partial T}{\partial x} + \frac{v_l}{\delta} \frac{\partial T}{\partial \eta} = \frac{\alpha_l}{\delta^2} \frac{\partial^2 T}{\partial \eta^2} \tag{3.35}$$

The interfacial conditions given by Eq.(3.26) and (3.28) can be rewritten respectively as;

$$\frac{\mu_l}{\delta} \frac{\partial u_l}{\partial \eta} = \mu_v \frac{\partial u_v}{\partial y} \tag{3.36}$$

$$v_v = - \frac{k_l}{h_{fg} \rho_v \delta} \left(\frac{\partial T}{\partial \eta}\right)_{\eta=0} + u_v \frac{d\delta}{dx} \tag{3.37}$$

If the overall energy balance, Eq.(3.32), is rewritten in terms of the new variable η;

$$\int_0^1 \frac{\partial}{\partial x}(r u_l \delta) dy = \frac{k_l}{h_{fg} \rho_l \delta} r \left(\frac{\partial T}{\partial \eta}\right)_{\eta=0} \tag{3.38}$$

This Eq. can be rearranged as;

$$\int_0^1 r u_l \left(\frac{d\delta}{dx}\right) d\eta + \int_0^1 r \delta \left(\frac{\partial u_l}{\partial x}\right) d\eta + \int_0^1 \delta u_l \left(\frac{dr}{dx}\right) d\eta = \frac{k_l}{h_{fg} \rho_l \delta} r \left(\frac{\partial T}{\partial \eta}\right)_{\eta=0} \tag{3.39}$$

CHAPTER 4

DISCRETIZATION

For the model considered, the finite difference shown in Figure 4.1 is used.

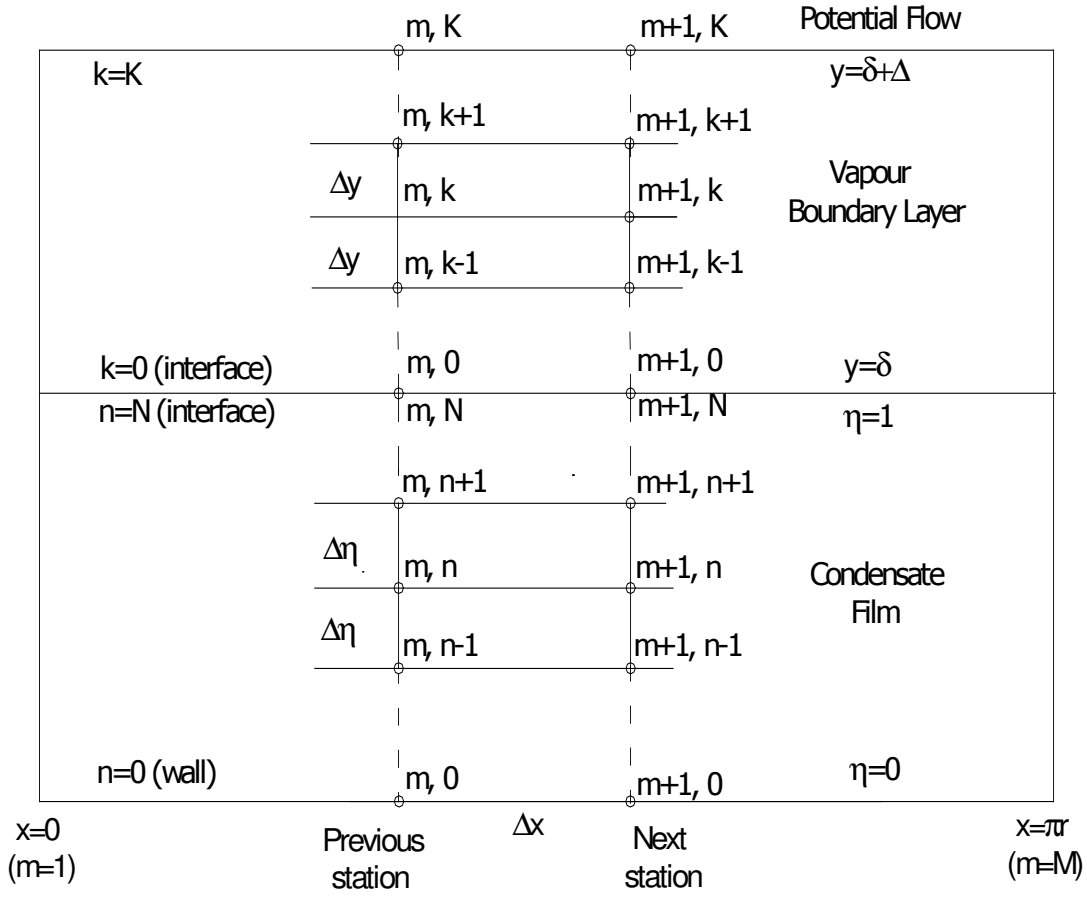

Figure 4.1 Finite-Difference Mesh for the Model

4.1. For the Liquid Boundary Layer

4.1.1. Momentum Equation

The following finite difference formulas, according to [4], were used to model $\partial u_l/\partial x$, $\partial u_l/\partial \eta$, $\partial^2 u_l/\partial \eta^2$;

$$\frac{\partial u_l}{\partial x} = \frac{(u_l)_{m+1,n} - (u_l)_{m,n}}{\Delta x} \qquad \text{(forward)}$$

$$\frac{\partial u_l}{\partial \eta} = \frac{(u_l)_{m,n+1} - (u_l)_{m,n-1}}{2\Delta \eta} \qquad \text{(central)}$$

$$\frac{\partial^2 u_l}{\partial \eta^2} = \frac{(u_l)_{m+1,n+1} - 2(u_l)_{m+1,n} + (u_l)_{m+1,n-1}}{\Delta \eta^2} \qquad \text{(central)}$$

If these are substituted into Eq.(3.34), the following relation can be obtained.

$$(u_l)_{m,n}\frac{(u_l)_{m+1,n} - (u_l)_{m,n}}{\Delta x} + \frac{(v_l)_{m,n}}{\delta_m}\frac{(u_l)_{m,n+1} - (u_l)_{m,n-1}}{2\Delta \eta} = \ldots$$

$$= \frac{\rho_v}{\rho_l}\frac{U^2_{v,m+1} - U^2_{v,m}}{2\Delta \eta} + \frac{\upsilon_l}{\delta_{m+1}{}^2}\frac{(u_l)_{m+1,n+1} - 2(u_l)_{m+1,n} + (u_l)_{m+1,n-1}}{\Delta \eta^2} + g\sin\left(\frac{x}{r_o}\right)$$

If this relation is rearranged;

$$(1+2\alpha_n)(u_l)_{m+1,n} = \alpha_n (u_l)_{m+1,n+1} + \alpha_n (u_l)_{m+1,n-1} + C_n \qquad (4.1)$$

where;

$$\alpha_n = \frac{\upsilon_l \Delta x}{\delta_m^2 (u_l)_{m,n} \Delta \eta^2} \qquad (4.2)$$

$$C_n = (u_l)_{m,n} - \frac{(v_l)_{m,n}\,\Delta x}{2(u_l)_{m,n}\,\delta_m\,\Delta\eta}\left((u_l)_{m,n+1} - (u_l)_{m,n-1}\right) + \frac{\rho_v}{\rho_l}\frac{U^2_{v,m+1} - U^2_{v,m}}{2(u_l)_{m,n}} + ..$$

$$+ \frac{g\sin\left(\frac{x}{r_o}\right)\Delta x}{(u_l)_{m,n}} \qquad (4.3)$$

4.1.2. Continuity Equation

According to [4], the following finite difference formulas were used to model $\partial u_l/\partial x$, $\partial v_l/\partial \eta$;

$$\frac{\partial u_l}{\partial x} = \frac{(u_l)_{m+1,n} - (u_l)_{m,n}}{\Delta x} \qquad \text{(forward)}$$

$$\frac{\partial v_l}{\partial \eta} = \frac{(v_l)_{m+1,n} - (v_l)_{m+1,n-1}}{\Delta \eta} \qquad \text{(backward)}$$

Putting these into the continuity equation, Eq.(3.33), and solving for the next vertical velocity:

$$(v_l)_{m+1,n} = (v_l)_{m+1,n-1} - \frac{\Delta\eta\,\delta_{m+1}}{2\Delta x\, r_{m+1}}\left\{r_{m+1}\left[(u_l)_{m+1,n} + (u_l)_{m+1,n-1}\right] - r_m\left[(u_l)_{m,n} + (u_l)_{m,n-1}\right]\right\} \qquad (4.4)$$

Once the u's and δ's for the next station (m+1) are known, next column of v's can be computed with this relation.

4.1.3. Energy Equation

If similar models for $\partial T/\partial x$, $\partial T/\partial \eta$, $\partial^2 T/\partial \eta^2$ as for to the momentum equation are used, the following equation can be obtained;

$$(u_l)_{m,n}\frac{T_{m+1,n}-T_{m,n}}{\Delta x}+\frac{(v_l)_{m,n}}{\delta_m}\frac{T_{m,n+1}-T_{m,n-1}}{2\Delta\eta}=\frac{\alpha_l}{\delta_{m+1}^2}\frac{T_{m+1,n+1}-2T_{m+1,n}+T_{m+1,n-1}}{\Delta\eta^2}$$

Solving for the next vertical temperature;

$$(1+2\beta_n)T_{m+1,n}=\beta_n T_{m+1,n+1}+\beta_n T_{m+1,n-1}+F_n \tag{4.5}$$

where

$$F_n=T_{m,n}-\frac{(v_l)_{m,n}\Delta x}{2(u_l)_{m,n}\delta_m\Delta y}\left(T_{m,n+1}-T_{m,n-1}\right) \tag{4.6}$$

$$\beta_n=\frac{\alpha_l\Delta x}{\delta_{m+1}^2(u_l)_{m,n}\Delta\eta^2} \tag{4.7}$$

4.2. For the Vapor Boundary Layer

4.2.1. Momentum Equation

Same finite difference procedure as for the liquid layer is applied:

$$(u_v)_{m,k}\frac{(u_v)_{m+1,k}-(u_v)_{m,k}}{\Delta x}+(v_v)_{m,k}\frac{(u_v)_{m,k+1}-(u_v)_{m,k-1}}{2\Delta y}=\ldots$$

$$=\frac{U^2_{v,m+1}-U^2_{v,m}}{2\Delta x}+\upsilon_v\frac{(u_v)_{m+1,k+1}-2(u_v)_{m+1,k}+(u_v)_{m+1,k-1}}{\Delta y^2}$$

If this relation is rearranged;

$$(1+2\gamma_n)(u_v)_{m+1,k} = \gamma_n (u_v)_{m+1,k+1} + \gamma_n (u_v)_{m+1,k-1} + E_k \quad (4.8)$$

where

$$E_k = (u_v)_{m,k} - \frac{(v_v)_{m,k}\,\Delta x}{2(u_v)_{m,k}\,\Delta y}\left((u_v)_{m,k+1} - (u_v)_{m,k-1}\right) + \frac{U^2_{v,m+1} - U^2_{v,m}}{2(u_l)_{m,k}} \quad (4.9)$$

$$\gamma_n = \frac{\upsilon_v\,\Delta x}{(u_{vl})_{m,k}\,\Delta y^2} \quad (4.10)$$

4.2.2. Continuity Equation

Same finite difference procedure is applied as for the liquid layer and the following next vertical velocity is obtained:

$$(v_v)_{m+1,k} = (v_v)_{m+1,k-1} - \frac{\Delta y}{2\Delta x\, r_{m+1}}\left\{r_{m+1}\left[(u_v)_{m+1,k} + (u_v)_{m+1,k-1}\right] - r_m\left[(u_v)_{m,k} + (u_v)_{m,k-1}\right]\right\} \quad (4.11)$$

4.3. Discretization of the Energy Balance and Interfacial Conditions

4.3.1. Energy Balance

The terms in the energy balance equation, Eq.(3.39), are discretized as follows;

$$\frac{d\delta}{dx} = \frac{\delta_{m+1} - \delta_m}{\Delta x} \qquad \text{(forward)}$$

$$\frac{\partial u_l}{\partial x} = \frac{(u_l)_{m+1,n} - (u_l)_{m,n}}{\Delta x} \qquad \text{(forward)}$$

$$\frac{dr}{dx} = \frac{r_{m+1,n} - r_{m,n}}{\Delta x} \qquad \text{(forward)}$$

Substituting these in the normalized energy balance, Eq.(3.39), and rearranging:

$$\delta_{m+1}\left[\frac{r_{m+1}}{\Delta x}\int_0^1 (u_l)_{m+1,n}\,d\eta + \frac{r_{m+1}}{\Delta x}\int_0^1 [(u_l)_{m+1,n} - (u_l)_{m,n}]d\eta + \frac{(r_{m+1}-r_m)}{\Delta x}\int_0^1 (u_l)_{m+1,n}\,d\eta\right] = ..$$

$$= \frac{k_l}{h_{fg}\,\rho_l\,\delta_m} r_m \left(\frac{\partial T_m}{\partial \eta}\right)_{\eta=0} + \delta_m \frac{r_{m+1}}{\Delta x}\int_0^1 (u_l)_{m+1,n}\,d\eta \qquad (4.12)$$

The integrals in Eq.(4.12) can be written as:

$$\int_0^1 (u_l)_{m,n}\,d\eta = \sum_0^{N-1}[(u_l)_{m,n+1} + (u_l)_{m,n}]\frac{\Delta\eta}{2}$$

$$\int_0^1 [(u_l)_{m+1,n} - (u_l)_{m,n}]d\eta = \sum_0^{N-1}[(u_l)_{m+1,n+1} + (u_l)_{m+1,n} - (u_l)_{m,n+1} - (u_l)_{m,n}]\frac{\Delta\eta}{2}$$

Substituting these in Eq.(4.12), rearranging and solving for δ_{m+1}:

$$\delta_{m+1} = \frac{\frac{2\,\Delta x\,k_l}{h_{fg}\,\rho_l\,\delta_m\,\Delta\eta} r_m \left(\frac{\partial T_m}{\partial \eta}\right)_{\eta=0} + \delta_m r_{m+1}\sum_0^{N-1}[(u_l)_{m+1,n+1} + (u_l)_{m+1,n}]}{\left[\begin{array}{l} 3r_{m+1}\sum_0^{N-1}[(u_l)_{m+1,n+1} + (u_l)_{m+1,n}] - r_{m+1}\sum_0^{N-1}[(u_l)_{m,n+1} + (u_l)_{m,n}] - ... \\ - r_m\sum_0^{N-1}[(u_l)_{m+1,n+1} + (u_l)_{m+1,n}] \end{array}\right]} \qquad (4.13)$$

4.3.2. Interfacial Conditions

The interfacial condition of the shear balance, Eq.(3.36) is discretized by a backward difference for the liquid velocity and a forward difference for the vapor velocity as follows;

$$\frac{\partial u_l}{\partial \eta} = \frac{(u_l)_{m+1,\delta} - (u_l)_{m+1,\delta-\Delta\eta}}{\Delta\eta} = \frac{(u_l)_{m+1,N} - (u_l)_{m+1,N-1}}{\Delta\eta}$$

$$\frac{\partial u_v}{\partial y} = \frac{(u_v)_{m+1,\delta+\Delta y} - (u_v)_{m+1,\delta}}{\Delta y} = \frac{(u_v)_{m+1,1} - (u_v)_{m+1,0}}{\Delta y}$$

$$\Rightarrow \quad (u_l)_{m+1,N} = (u_v)_{m+1,0} = \frac{\frac{\delta_m \mu_v \Delta\eta}{\mu_l \Delta y}(u_v)_{m+1,1} + (u_l)_{m+1,N-1}}{1 + \frac{\delta_m \mu_v \Delta\eta}{\mu_l \Delta y}} \tag{4.14}$$

And the interfacial condition given by Eq.(3.37) is discretized by a forward difference for δ as follows;

$$\frac{\partial \delta}{\partial x} = \frac{\delta_{m+1} - \delta_m}{\Delta x}$$

Where δ_{m+1} is given by Eq.(4.13). After substitution and rearranging;

$$(v_v)_{m+1,\delta} = -\frac{k_l}{h_{fg}\,\rho_v \delta_{m+1}} \left(\frac{\partial T_{m+1}}{\partial \eta}\right)_{\eta=0} + (u_v)_{m+1,\delta} \frac{\delta_{m+1} - \delta_m}{\Delta x} \tag{4.15}$$

CHAPTER 5

CALCULATION OF THE FIRST GRID LINE

Since in the stagnation region the flow velocity is small, we can consider the flow as creeping flow and neglect the inertia terms and the pressure gradient in the momentum equation for the condensate layer. Eq.(3.34) in this form can be written as:

$$\frac{\upsilon_l}{\delta^2}\frac{\partial^2 u_l}{\partial \eta^2} = g\sin\left(\frac{x}{r_o}\right) \tag{5.1}$$

Since x/r_o is very small Eq.(5.1) becomes;

$$\frac{\upsilon_l}{\delta^2}\frac{\partial^2 u_l}{\partial \eta^2} = g\frac{x}{r_o}$$

$$\Rightarrow\ u_l = -\frac{g\delta^2 x}{2\upsilon_l r_o}\eta^2 + c_1\eta + c_2$$

$$\eta = 0\ ;\ u_l = 0 \ \Rightarrow\ c_1 = 0$$

$$\eta = 1\ ;\ \frac{\partial u_l}{\partial \eta} = 0 \ \Rightarrow\ c_1 = \frac{g\delta^2 x}{\upsilon_l r_o}$$

$$\Rightarrow\ u_l = \frac{g\delta^2 x}{\upsilon_l r_o}\left(\eta - \frac{\eta^2}{2}\right) \tag{5.2}$$

If we substitute this into the energy balance, Eq.(3.31), the liquid film thickness, δ, at the first grid line can be calculated as;

$$\delta = \left[\frac{3}{2} \frac{\upsilon_l r_0 k_l (T_S - T_W)}{h_{fg} \rho_l g} \right]^{1/4} \tag{5.3}$$

The y-velocities in the liquid can be found by substituting u_l, Eq.(5.2), into the continuity equation, Eq.(3.33);

$$v_l = \frac{2g\delta^3}{\upsilon_l r_0} \left(\frac{\eta^3}{6} - \frac{\eta^2}{2} \right) \tag{5.4}$$

The temperature profile can be assumed linear and can be found as follows:

$$T = (T_s - T_w)\eta + T_w \tag{5.5}$$

Since the velocities are very small in the upper stagnation region, the velocities of vapor can be assumed to be those of the liquid at the interface:

$$u_v = (u_l)_\delta \tag{5.6}$$

$$v_v = (v_l)_\delta \tag{5.7}$$

CHAPTER 6

NUMERICAL PROCEDURE

6.1. Calculation of the x-Velocities

To calculate the x-velocities; the velocity Eqs.; Eq.(4.1) and (4.5), the interfacial condition, Eq.(4.14), and the boundary conditions; Eq.(3.9) and (3.16) are used. These combined system can be solved by a procedure, called the tridiagonal matrix algorithm [4]. Using this algorithm, the back-substitution recurrence relation of Eq.(4.1) has the form:

$$(u_l)_{n-1} = P_{n-1}(u_l)_n + Q_{n-1} \tag{6.1}$$

At the bottom of the liquid film (n=0), u_l=0. Thus from Eq.(4.1) we get:

$$P_1 = \frac{\alpha_1}{1+2\alpha_1} \tag{6.2}$$

$$Q_1 = \frac{C_1}{1+2\alpha_1} \tag{6.3}$$

To calculate the remaining *P*'s and *Q*'s, Eq.(4.1) and (6.1) are combined, and the following recurrence relations are obtained:

$$P_n = \frac{\alpha_n}{1+2\alpha_n - \alpha_n P_{n-1}} \tag{6.4}$$

$$Q_n = \frac{C_n + \alpha_n Q_{n-1}}{1 + 2\alpha_n - \alpha_n P_{n-1}} \tag{6.5}$$

The back-substitution recurrence relation for of Eq.(4.8) has the form;

$$(u_v)_{k-1} = PV_{k-1}(u_v)_k + QV_{k-1} \tag{6.6}$$

One Equality of Eq.(4.1) is:

$$(u_l)_{N-1} = P_{N-1}(u_l)_N + Q_{N-1} \tag{6.7}$$

At the top of the liquid film (n=N), the interfacial condition, Eq.(4.14), exists. If Eq.(6.7) is substituted into Eq.(4.14), and the resulting equation is solved for $(u_v)_0$:

$$(u_v)_o = \frac{\frac{\delta_m \mu_v \Delta\eta}{\mu_l \Delta y}}{1 + \frac{\delta_m \mu_v \Delta\eta}{\mu_l \Delta y} - P_{n-1}}(u_v)_1 + \frac{Q_{N-1}}{1 + \frac{\delta_m \mu_v \Delta\eta}{\mu_l \Delta y} - P_{N-1}} \tag{6.8}$$

It can be seen from the back-substitution recurrence relation for vapor, Eq.(6.6);

$$PV_o = \frac{\frac{\delta_m \mu_v \Delta\eta}{\mu_l \Delta y}}{1 + \frac{\delta_m \mu_v \Delta\eta}{\mu_l \Delta y} - P_{N-1}} \tag{6.9}$$

$$QV_0 = \frac{Q_N}{1 + \frac{\delta_m \mu_v \Delta\eta}{\mu_l \Delta y} - P_{N-1}} \tag{6.10}$$

To calculate the remaining *P*'s and *Q*'s, Eq.(4.8) and (6.6) are combined, and the following recurrence relations are obtained:

$$PV_k = \frac{\gamma_k}{1 + 2\gamma_k - \gamma_k PV_{k-1}} \tag{6.11}$$

$$QV_k = \frac{E_k + \gamma_k QV_{k-1}}{1 + 2\gamma_k - \gamma_k PV_{k-1}} \tag{6.12}$$

At k=K the vapor x-velocity is equal to the potential flow velocity. Since all PV's and QV's are known, using the back-substitution recurrence relation for vapor, Eq.(6.6), the x-velocity at k=K-1 is calculated. The way is worked down up to the interface where k=0 or n=N. Knowing the liquid x-velocity at n=N, we work our way down using the back-substitution recurrence relation for liquid, Eq.(6.1). Hence, all of the x-velocities at station m+1 for the vapor and for the liquid are calculated.

6.2. Calculation of the Film Thickness (δ)

Since the x-velocities at station m+1 are known, the film thickness (δ) at station m+1 can be calculated using Eq.(4.13).

6.3. Calculation of the Temperature

The back-substitution recurrence relation of the energy equation, Eq.(4.1), has the form:

$$T_{n-1} = PT_{n-1} T_n + QT_{n-1} \tag{6.13}$$

At the bottom of the liquid film (n=0), $T=T_w$. Thus from Eq.(4.5) we get:

$$PT_1 = \frac{\beta_1}{1 + 2\beta_1} \tag{6.14}$$

$$QT_1 = \frac{\beta_1 T_w + F_1}{1 + 2\beta_1} \tag{6.15}$$

To calculate the remaining *P*'s and *Q*'s, Eq.(4.5) and (6.13) are combined, and the following recurrence relations are obtained:

$$PT_n = \frac{\beta_n}{1 + 2\beta_n - \beta_n PT_{n-1}} \tag{6.16}$$

$$QT_n = \frac{\beta_n QT_{n-1} + F_{n-1}}{1 + 2\beta_n - \beta_n PT_{n-1}} \tag{6.17}$$

At n=N the temperature is equal to the saturation temperature. Since all PV's and QV's are known, using the back-substitution recurrence relation, Eq.(6.13), the temperature at n=N-1 is calculated. The way is worked down up to n=1. Hence, all temperatures within the liquid at station m+1 are calculated.

6.4. Calculation of the y-Velocities

The y-velocity at y=0 is zero. Knowing this, with Eq.(4.4) the next condensate y-velocities up to the interface (y=N or k=0) are calculated. The y- velocity at the interface is calculated by Eq.(4.15). Using this velocity, with Eq.(4.11), going upward, the y-velocities of vapor are calculated. Hence, all of the y-velocities at station m+1 for the vapor and for the liquid are calculated.

6.5. Calculation of the Local Nusselt Number

The local Nusselt number can be calculated as follows:

$$Nu_x = \frac{h_x \cdot 2r_0}{k_l} \tag{6.18}$$

Where, the heat transfer coefficient is expressed as:

$$h_x = \frac{k \cdot \left(\frac{\partial T}{\partial y}\right)_{y=0}}{T_s - T_w} \tag{6.19}$$

6.6. Calculations for the Horizontal Cylinder

In the formulation of the problem, the difference for the horizontal cylinder is the distance of axis of symetry (r) and the potential flow velocity (U_Φ). If the width of the cylinder is taken as 1 meter, Eq.(3.7) and (3.16) can be written for the cylinder as:

$$r = 1\,m \tag{6.20}$$

$$U_v = 2\,U_\infty \sin\left(\frac{x}{r_o}\right) \tag{6.21}$$

CHAPTER 7

RESULTS

The formulation of laminar filmwise condensation of flowing vapor over a sphere was examined analytically up to this Chapter. In this Chapter, the results for the velocity distributions both in the condensate and vapor boundary layer, the location of the separation point, the temperature distribution in the condensate layer, the condensate film thickness and the local Nusselt number due to condensation of water vapor over the cold sphere are represented. The effect of pressure gradient, gravity, vapor oncoming velocity and sphere radius on these parameters are given, and the results for the flow over a sphere are compared with the flow over a circular cylinder. Finally, the results for mercury, which is a liquid metal, are obtained and compared with the results for water.

In this Chapter, just the results are represented. In Chapter 8, these results are discussed.

To get the relevant results, a computer program in MathCad was written. This computer program is given in Appendix A.

In the calculations for the flow over a cylinder, Eq. (6.20) and Eq. (6.21) were used instead of Eq. (3.7) and Eq. (3.16).

The calculations were made for water vapor flowing at saturated state except in 7.7. In this part, the calculations were made for mercury at saturated state.

The thermophysical constants for the liquid were taken as those at the average of the saturation and surface temperature. The thermophysical constants for water and the physical dimensions used in the computer program are:

T_s = 375 K (Saturation pressure at 1 atm. pressure)
T_w = 365 K
ρ_l = 961.8 kg/m^3
ρ_v = 0597 kg/m^3
ν_l = 0.31 x 10^{-6} m^2/s
ν_v = 0.02 x 10^{-3} m^2/s
μ_l = 0.298 x 10^{-3} kg/ms
μ_v = 1.255 x 10^{-5} kg/ms
k_l = 0.676 W/mK
h_{fg} = 2256.7 x 10^3 J/kg
C_p = 4210.7 J/kgK
r_o = 15 mm
Δx = 2.6 x 10^{-4} m
$\Delta \eta$ = 1 x 10^{-1}
Δy = 1 x 10^{-5} m

In the computer program, 180 equally spaced layers in x-direction (each 1 degree on the sphere), 10 equally spaced layers in η-direction for the condensate, and 250 equally spaced layers in y-direction for the vapor were taken.

In the formulation of the computer program, subscript f is used for liquid instead of l, and subscript g is used for vapor instead of v.

7.1. Liquid and Vapor Velocity Distributions

The graphical results for the velocity distribution of the liquid and condensate for an oncoming velocity of 20 m/s are shown in Figure 7.1. The data used here is given in Appendix B.1.

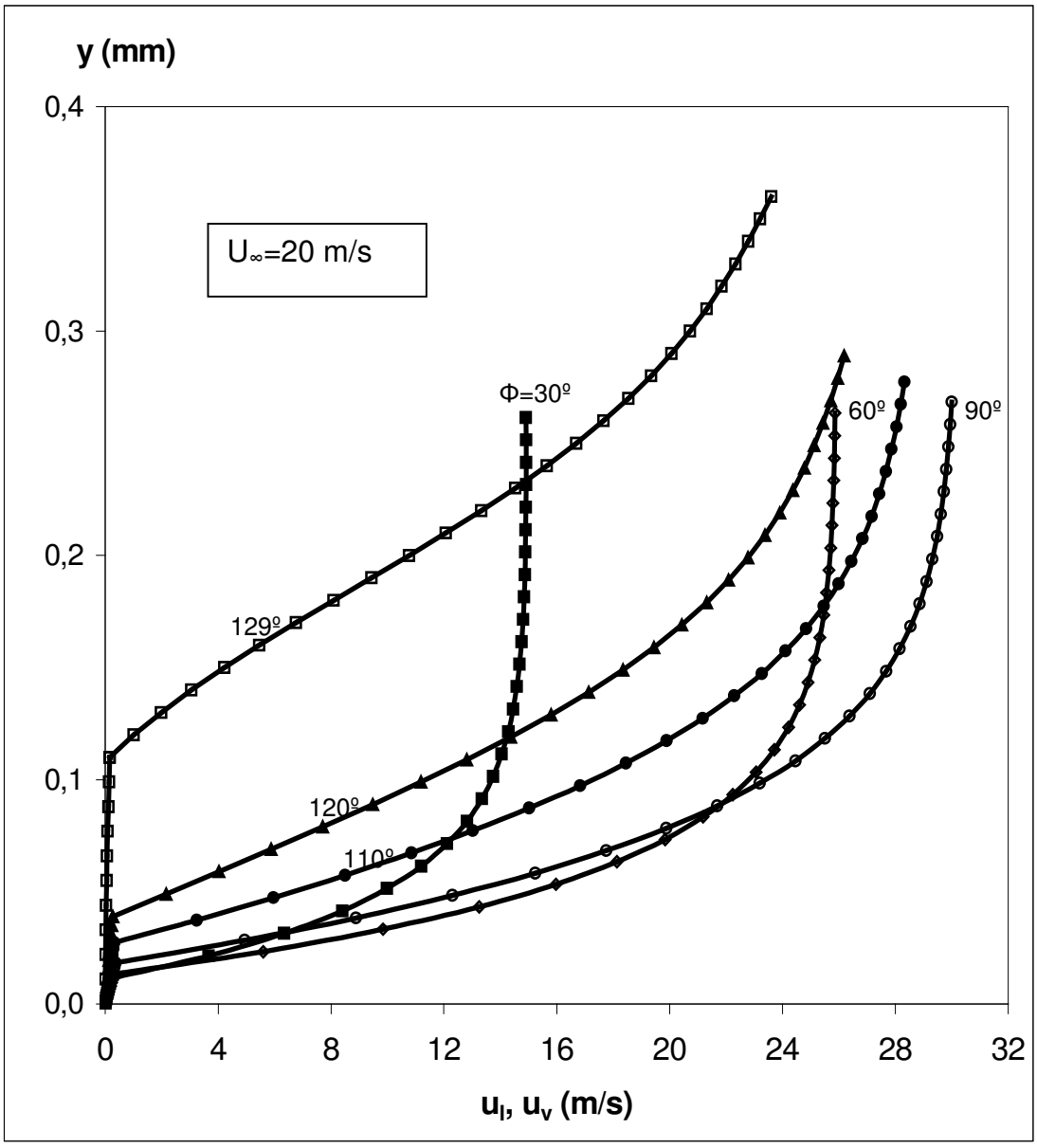

Figure 7.1. Velocity Profiles within the Condensate and Vapor - Linear Scale

In this linear scale graph, the liquid velocities cannot be observed. To observe also the liquid velocity distribution, a logarithmic scale graph is given in Figure 7.2.

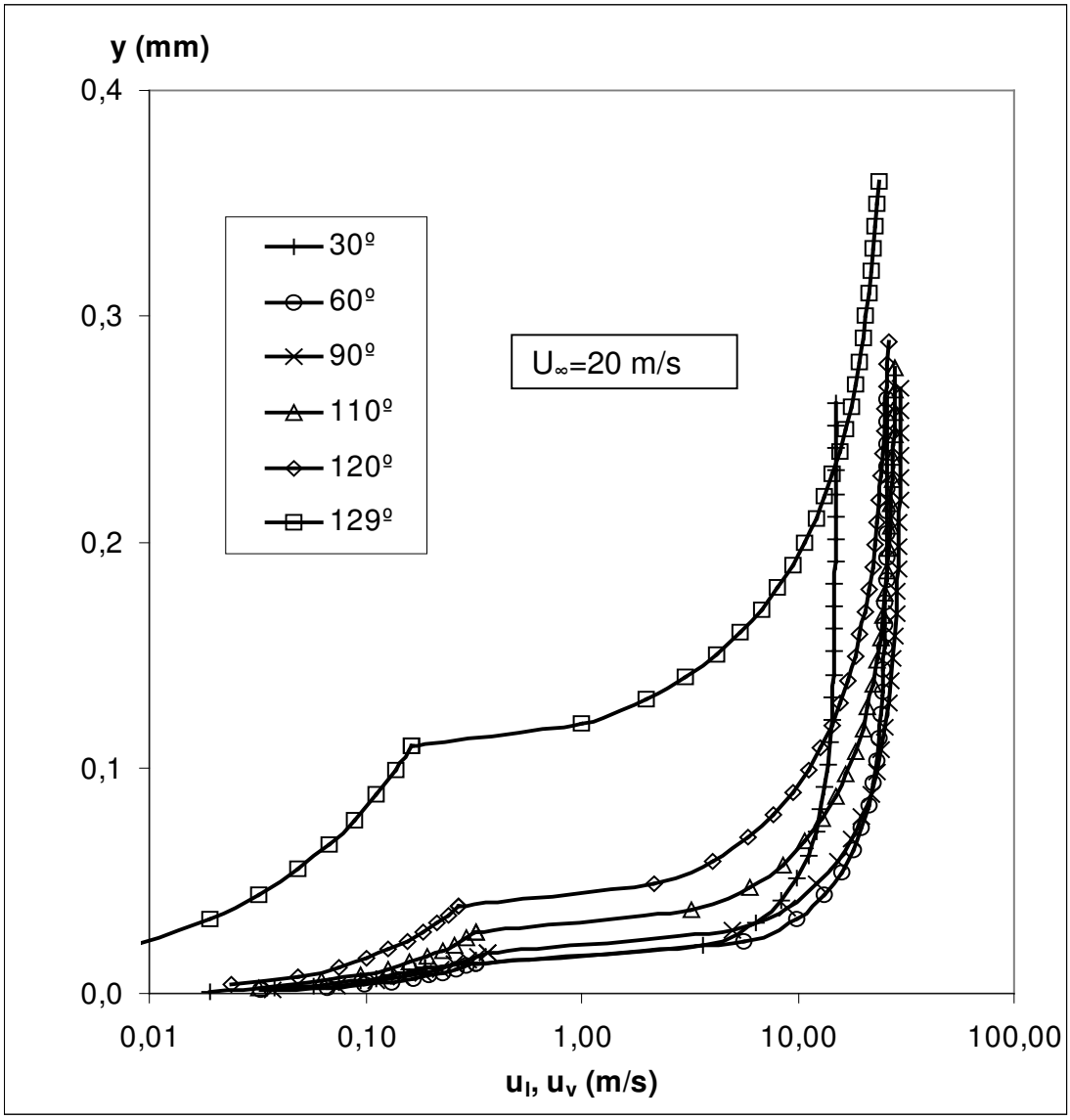

Figure 7.2. Velocity Profiles within the Condensate and Vapor - Logarithmic Scale

Velocity distribution results of the condensate with respect to the dimensionless film thickness, η, are given in Table 7.1. These are also shown as a diagram in Figure 7.3.

Table 7.1. Liquid Velocity Distribution (u in m/s, x in degree)

η	x→ 0	30	60	90	110	120	125	129	130
0	0	0,00	0,00	0,00	0,00	0,00	0,00	0,00	0,00
0,1	0	0,02	0,03	0,04	0,03	0,02	0,02	0,00	-0,01
0,2	0	0,04	0,07	0,07	0,06	0,05	0,04	0,01	-0,01
0,3	0	0,06	0,10	0,11	0,10	0,08	0,06	0,02	-0,01
0,4	0	0,08	0,13	0,15	0,13	0,10	0,08	0,03	0,00
0,5	0	0,10	0,17	0,19	0,16	0,13	0,10	0,05	0,01
0,6	0	0,11	0,20	0,22	0,19	0,16	0,12	0,07	0,03
0,7	0	0,13	0,23	0,26	0,23	0,18	0,15	0,09	0,06
0,8	0	0,15	0,26	0,30	0,26	0,21	0,17	0,11	0,08
0,9	0	0,17	0,30	0,33	0,29	0,24	0,20	0,14	0,11
1	0	0,19	0,33	0,37	0,33	0,27	0,23	0,16	0,14

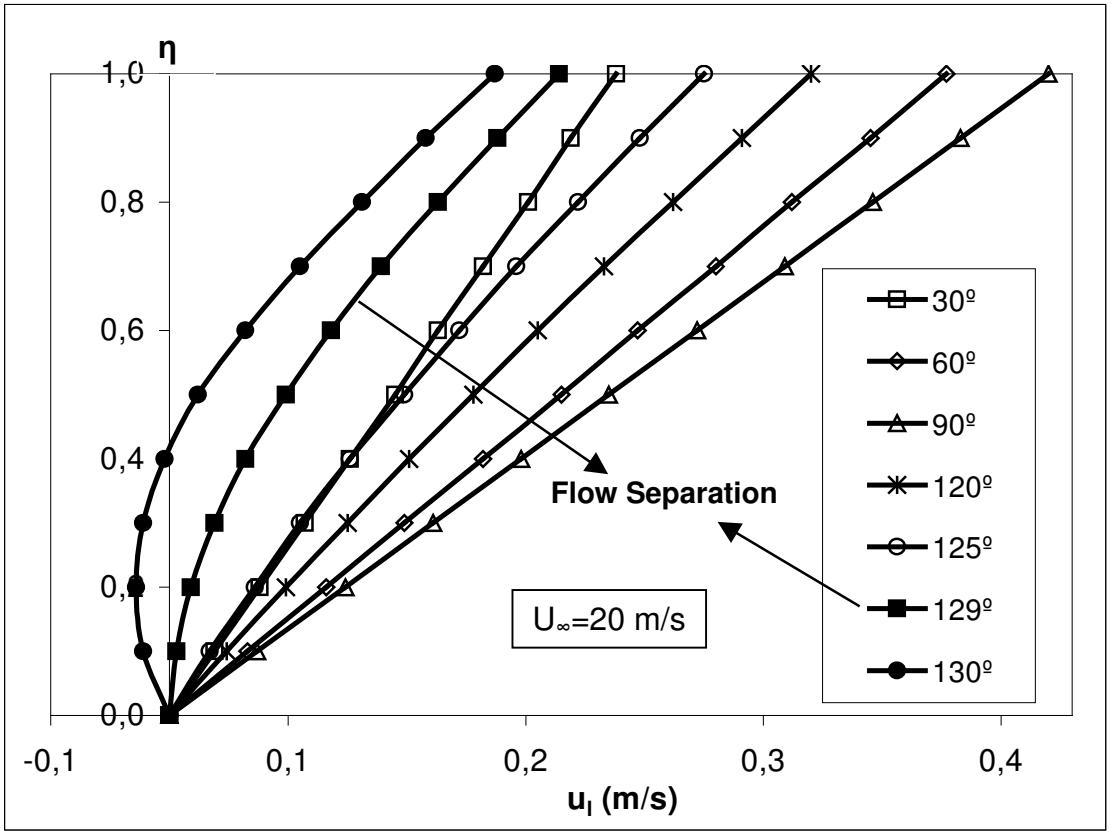

Figure 7.3. Velocity Profiles within the Condensate

7.2. Liquid Temperature Distribution

In Table 7.2., the temperature data within the condensate is given. The oncoming velocity was taken as 20 m/s.

Table 7.2. Liquid Temperature Distribution (T in K, x in degree)

η	$x \rightarrow 0$	30	60	90	120	130
0	0,00	365,00	365,00	365,00	365,00	365,00
0,1	0,00	366,00	366,00	366,00	365,98	364,74
0,2	0,00	367,01	367,00	367,00	366,96	366,04
0,3	0,00	368,01	368,01	368,00	367,95	367,21
0,4	0,00	369,01	369,01	369,00	368,94	368,33
0,5	0,00	370,01	370,01	370,00	369,94	369,42
0,6	0,00	371,01	371,01	371,00	370,94	370,50
0,7	0,00	372,01	372,01	372,00	371,95	371,58
0,8	0,00	373,01	373,00	373,00	372,96	372,67
0,9	0,00	374,00	374,00	374,00	373,98	373,77
1	0,00	375,00	375,00	375,00	375,00	375,00

The temperature distribution with the data given in Table 7.2. is shown in Figure 7.4.

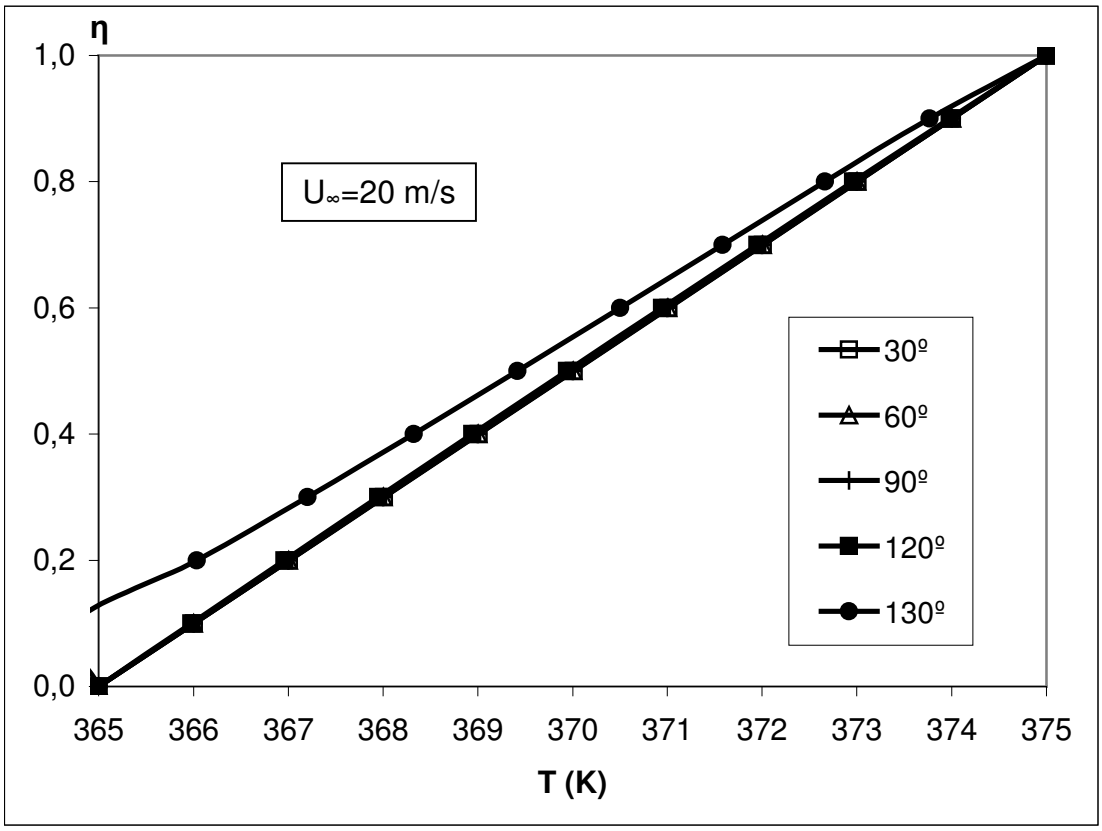

Figure 7.4. Temperature Distribution within the Condensate

7.3. Liquid Film Thickness

The variation of the liquid film thicknesses up to flow separation are investigated in three parts;

1. Variation with angular position at various oncoming velocities. (Figure 7.5.)
2. Variation with angular position with and without pressure gradient. (Figure7.6.- Pressure gradient in Eq.3.4. and Eq.3.8 was neglected)
3. Variation with angular position at normal gravity (g) and high gravity (100g) for two different oncoming velocities. (Figure 7.7.)

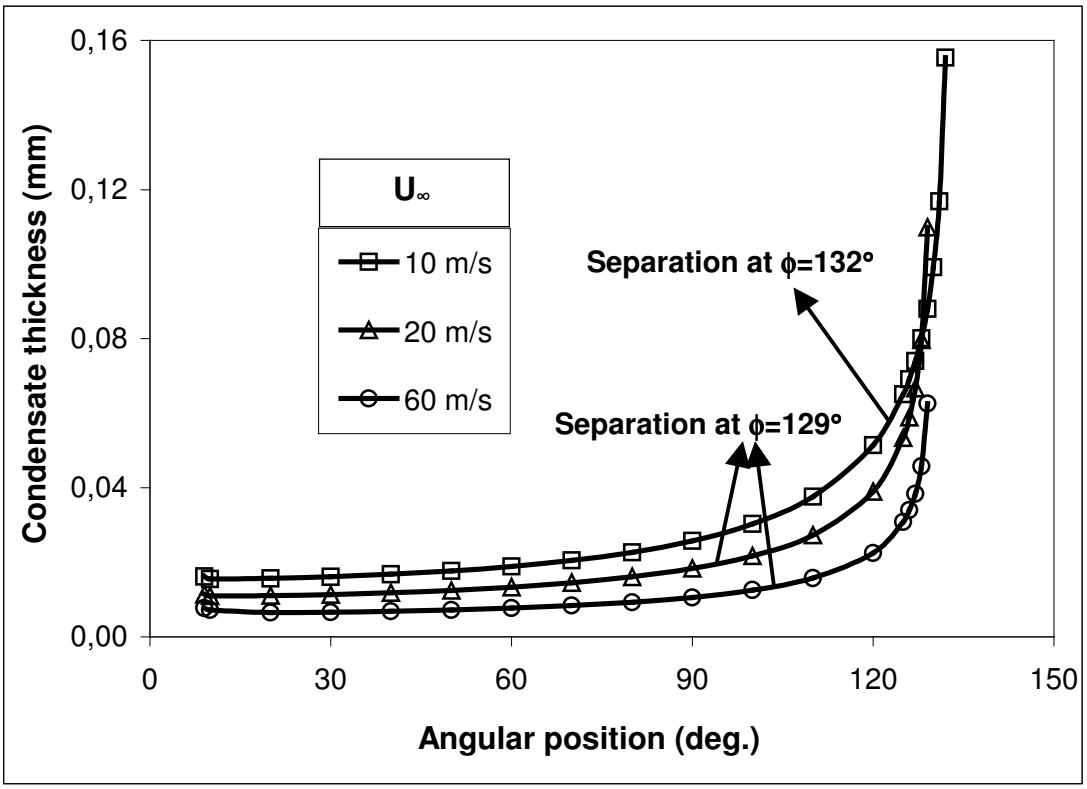

Figure 7.5. Condensate Thicknesses at Various Oncoming Velocities

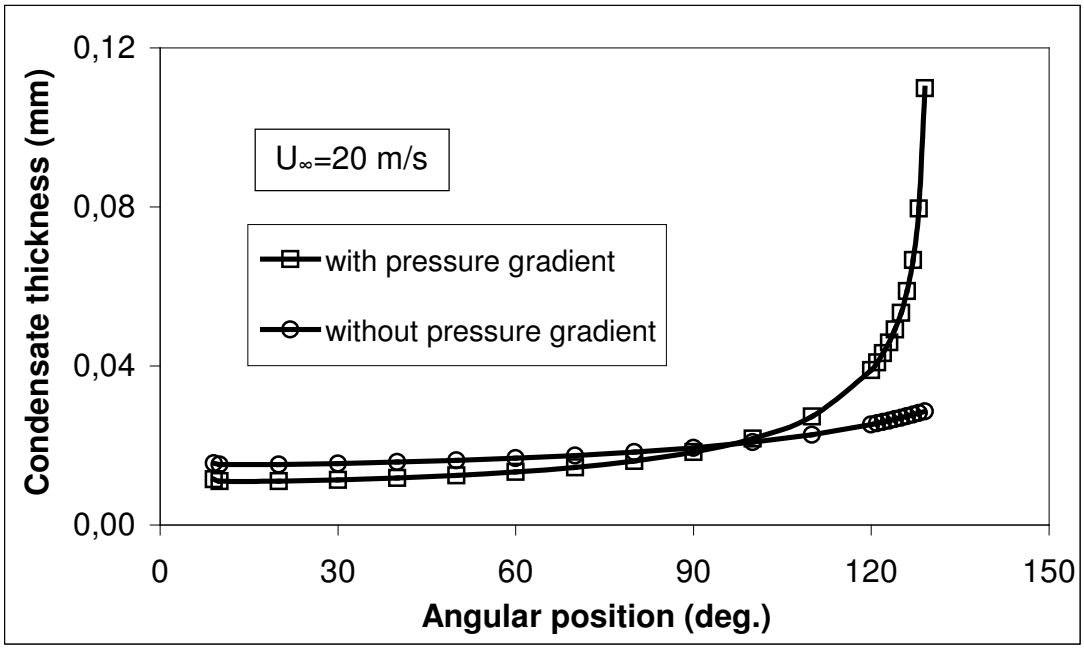

Figure 7.6 Effect of Pressure Gradient on Condensate Thickness (No flow separation without pressure gradient)

The data for the condensate thicknesses used in Figure 7.5. and Figure 7.6. are given in Appendix B.2 and Appendix B.3, respectively.

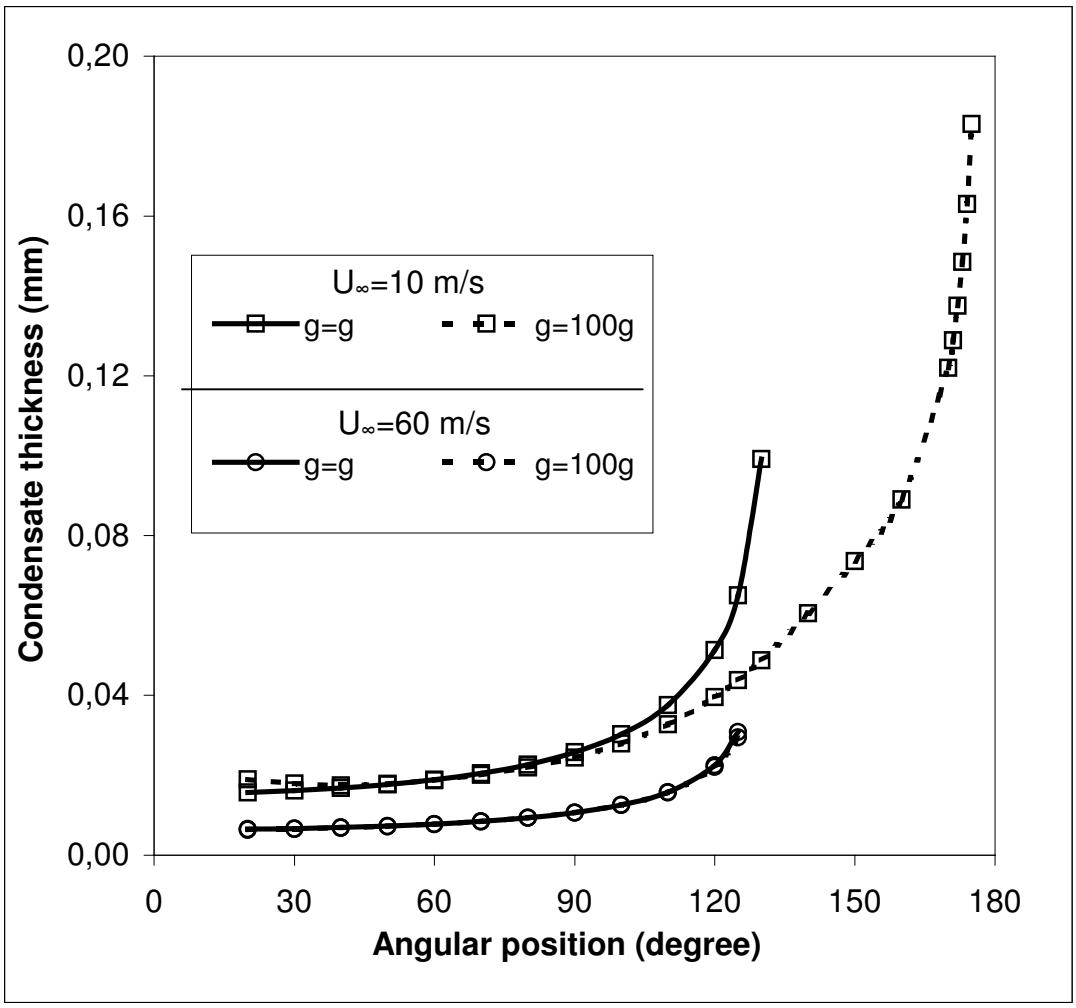

Figure 7.7. Variation of the Condensate Thickness with Gravity

7.4. Local Nusselt Number

The variation of the local Nusselt number at various oncoming velocities up to flow separation is shown in Figure 7.8. In the calculations, the oncoming velocities were taken as 10, 20 and 60 m/s, respectively.

The data used in Figure 7.8. is given in Appendix B.4.

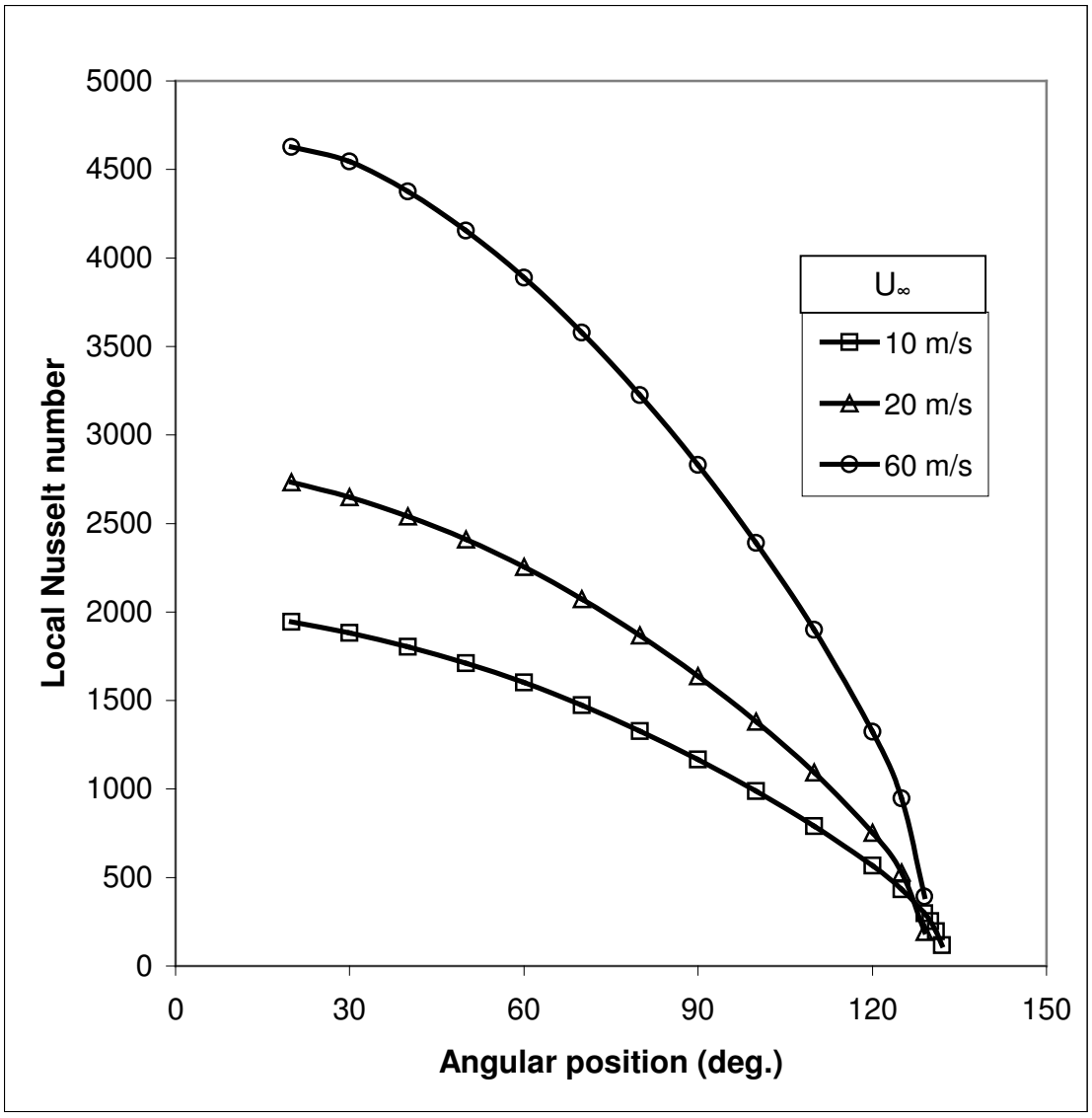

Figure 7.8. Variation of the Local Nusselt Number with Angular Position at Various Oncoming Velocities

Also the effect of pressure gradient on local Nusselt number is important. Therefore, the variation of the local Nusselt number with angular position with and without pressure gradient up to flow separation was determined. The results are shown in Figure 7.9. This graph represents the situation for an oncoming velocity of 20 m/s.

The data used in Figure 7.9. is given in Appendix B.5.

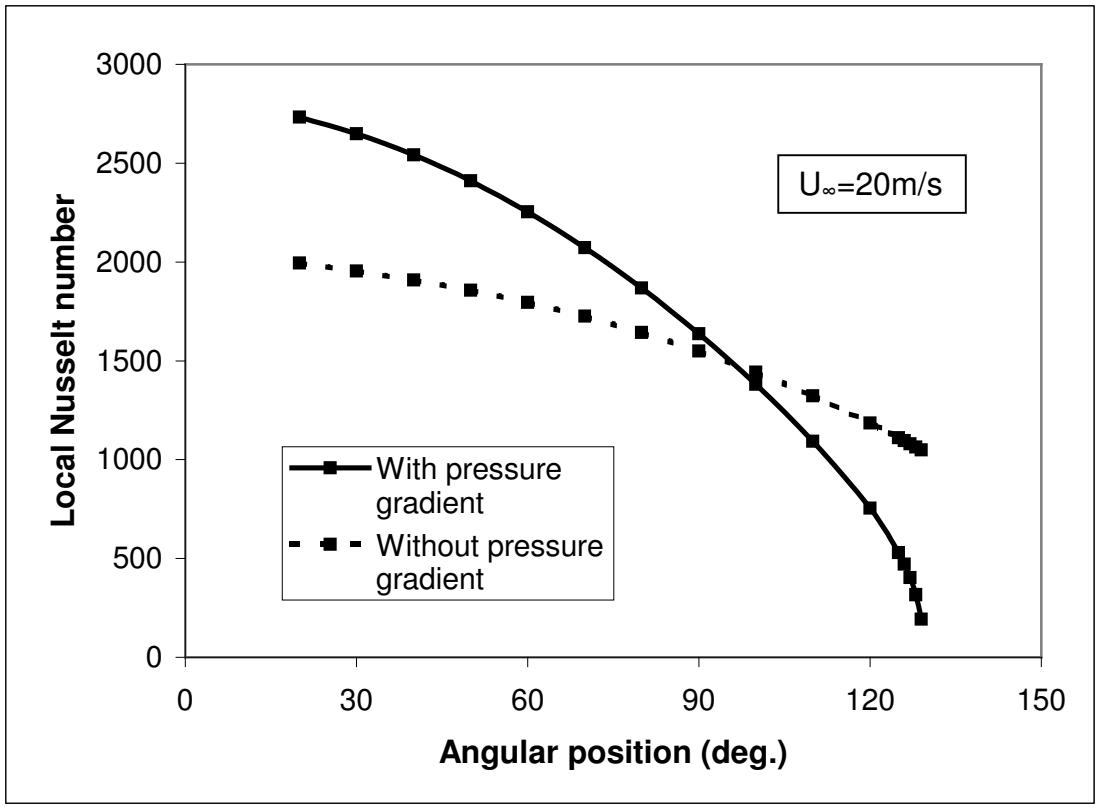

Figure 7.9. Variation of the Local Nusselt Number with Angular Position with and without Pressure Gradient

7.5. Results for the Cylinder

The results for the cylinder were obtained using Eq.(6.20) and Eq.(6.21) instead of Eq.(3.7) and Eq.(3.16). The results are compared with the results for the sphere including the following parameters:

1. Velocity profiles within the condensate. (Figure 7.10. and 7.11.)
2. Condensate film thickness up to flow separation. (Figure 7.12.)
3. Local Nusselt number up to flow separation. (Figure 7.13.)

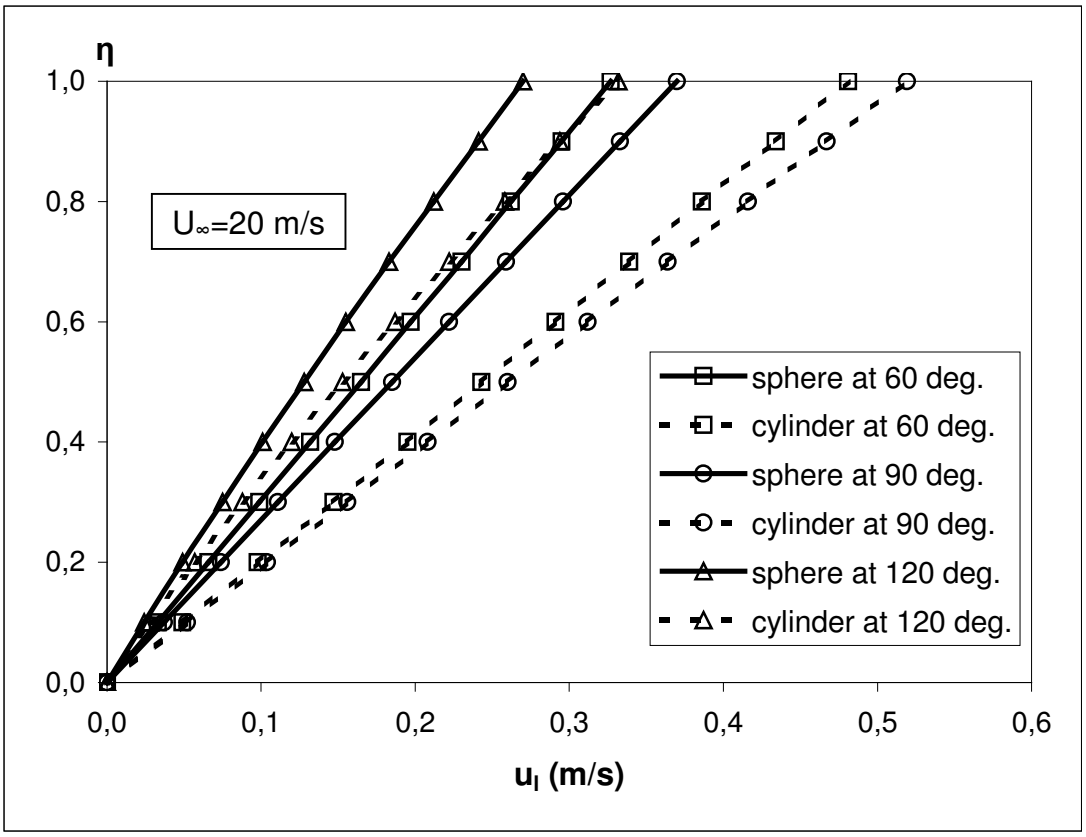

Figure 7.10. Comparison of the Condensate Velocity Profiles for the Sphere and Cylinder

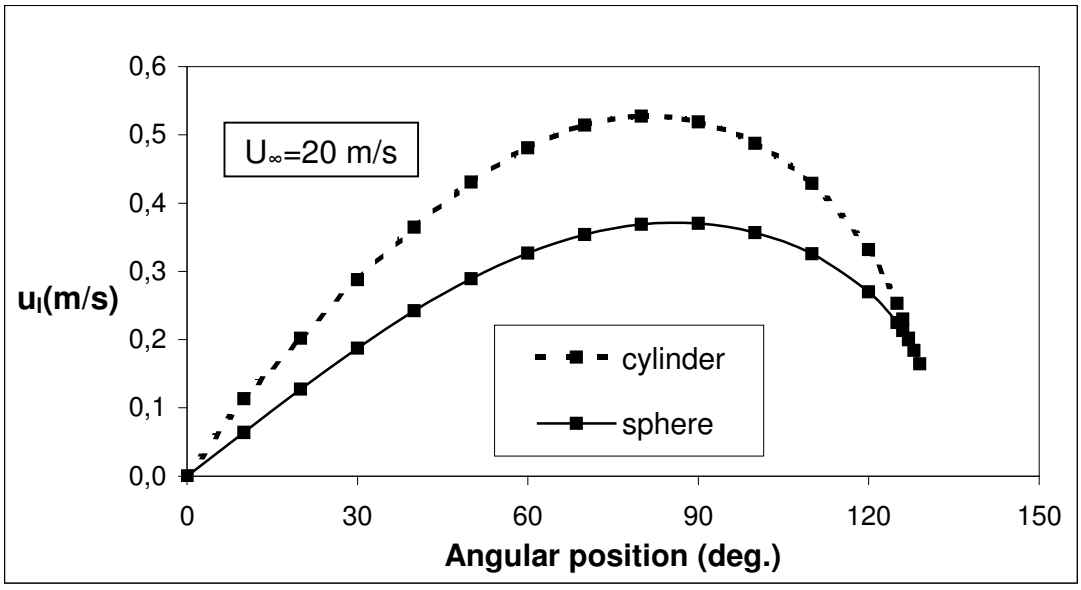

Figure 7.11. Comparison of the Velocity Profiles in the Condensate at η=1 for the Sphere and Cylinder

The data used in Figure 7.10. is given in Appendix B.6.

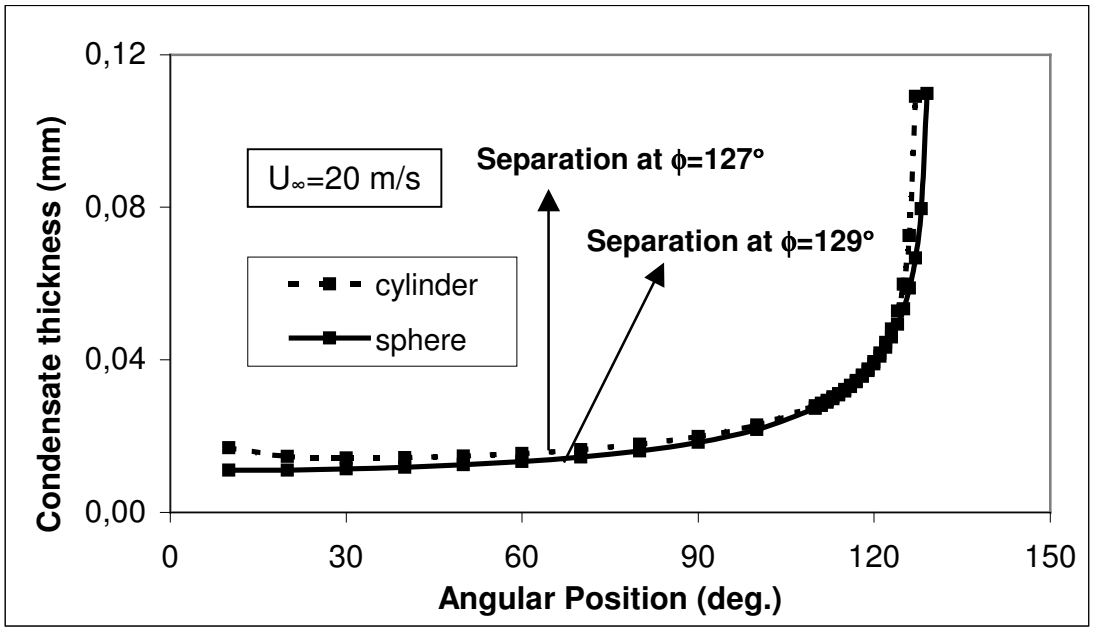

Figure 7.12. Comparison of the Condensate Thickness for the Sphere and Cylinder

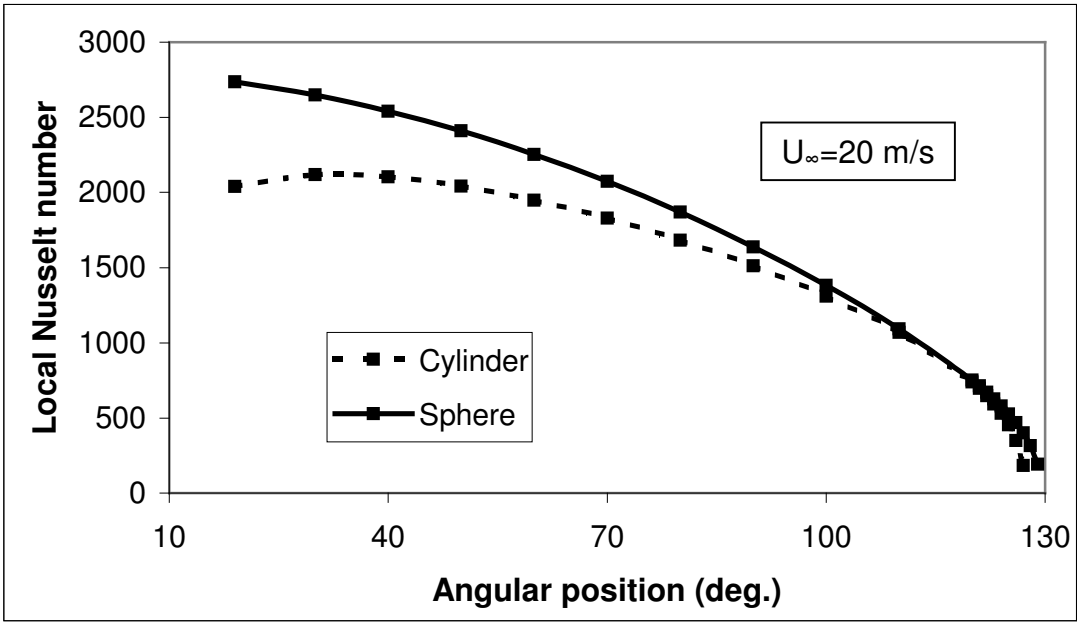

Figure 7.13. Comparison of the Local Nusselt Number for the Sphere and Cylinder

The data used in Figure 7.12. and Figure 7.13. is given in Appendix B.7.

7.6. Effect of the Sphere Radius

The effect of the sphere radius on condensate velocity (Figure 5.14), condensate film thickness (Figure 5.15.) and on the local Nusselt number (Figure 5.16.) up to flow separation is observed by increasing the sphere radius from 15 mm to 30 mm.

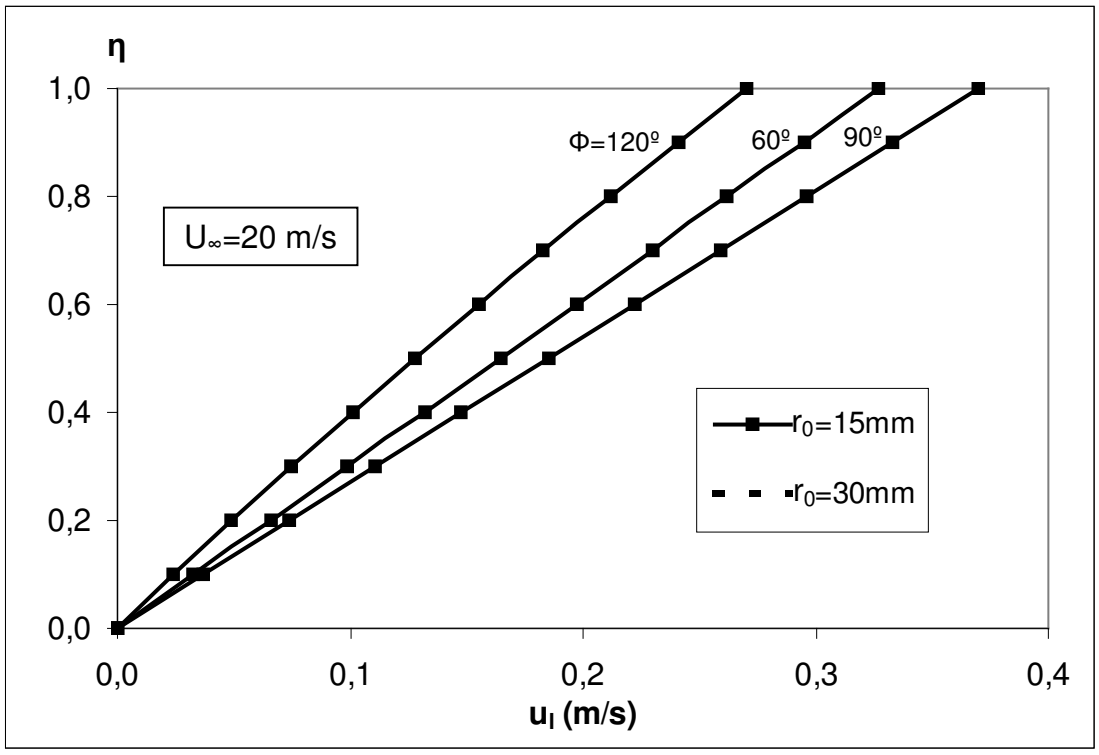

Figure 7.14. Effect of the Sphere Radius on Condensate Velocity Profile

The data used in Figure 7.14. is given in Appendix B.8.

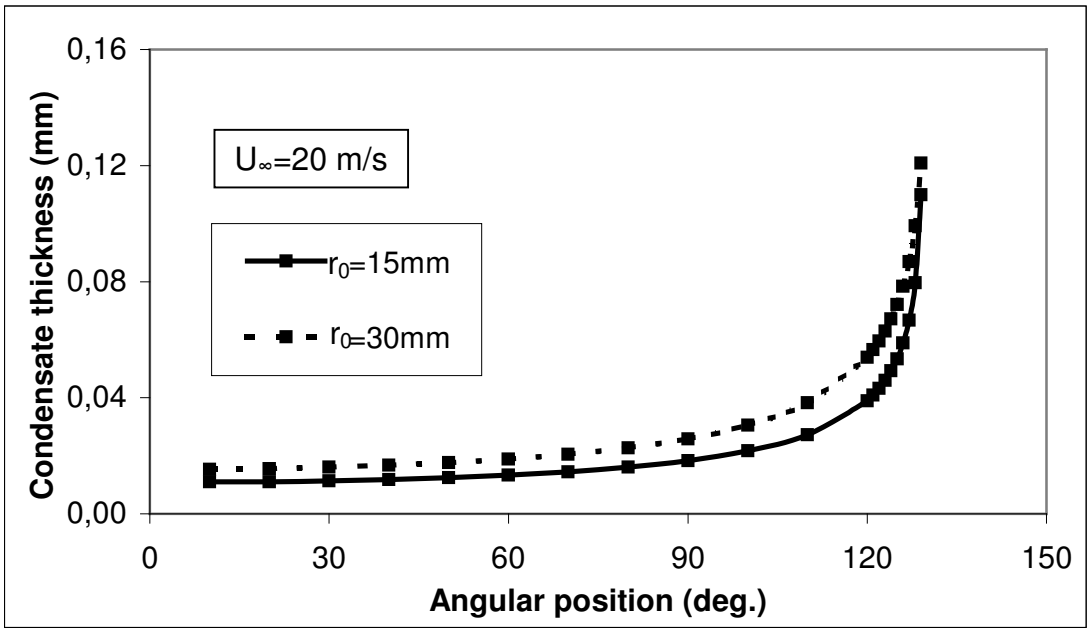

Figure 7.15. Comparison of the Condensate Thicknesses at Different Sphere Radii

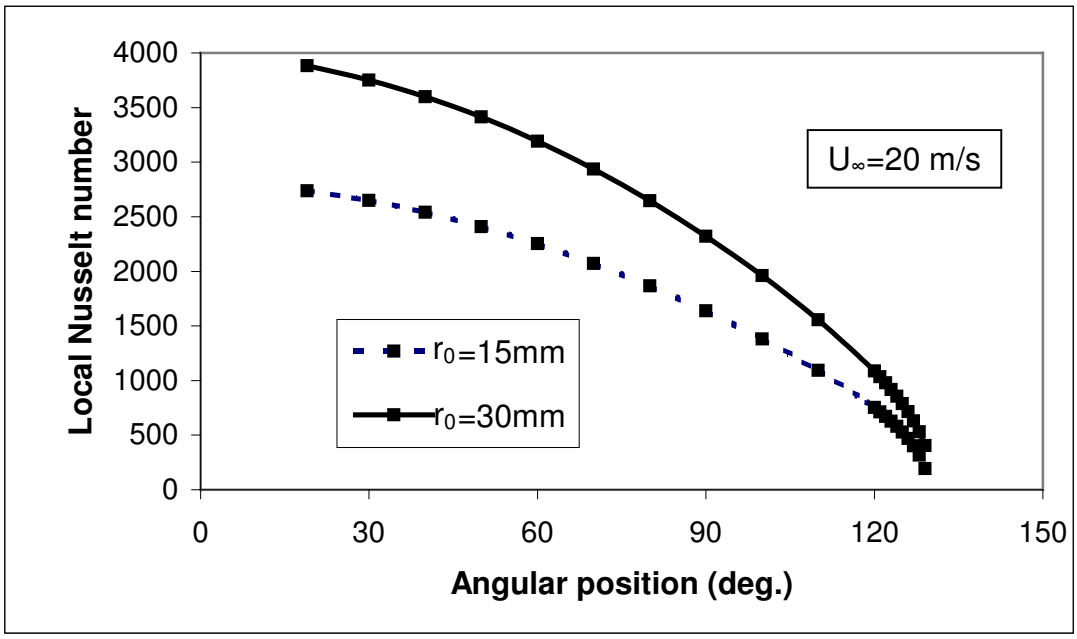

Figure 7.16. Effect of the Sphere Radius on the Local Nusselt Number

The data used in Figure 7.15. and Figure 7.16. is given in Appendix B.9.

7.7. Results for Mercury

For mercury, which is a liquid metal, the following thermophysical constants and physical dimensions were used in the computer program.

T_s = 630.1 K (Saturation temperature at 1 atm. pressure)
T_w = 620.1 K
ρ_l = 12750 kg/m^3
ρ_v = 3.91 kg/m^3
ν_l = 0.62 x 10^{-7} m^2/s
ν_v = 0.016 x 10^{-3} m^2/s
μ_l = 0.79 x 10^{-3} kg/ms
μ_v = 6.2 x 10^{-5} kg/ms
k_l = 14.57 W/mK
h_{fg} = 294.9 x 10^3 J/kg
C_p = 134 J/kgK
r_o = 15 mm
Δx = 2.6 x 10^{-4} m
$\Delta \eta$ = 1 x 10^{-1}
Δy = 1 x 10^{-5} m

The vapor properties of mercury were taken from the table given in Appendix B.10. The liquid state properties were taken from [19]. The results for mercury and water are compared by the following parameters:

1. Velocity profiles within the condensate. (Figure 7.17.)
2. Condensate film thickness up to flow separation. (Figure 7.18.)
3. Local Nusselt number up to flow separation. (Figure 7.19.)

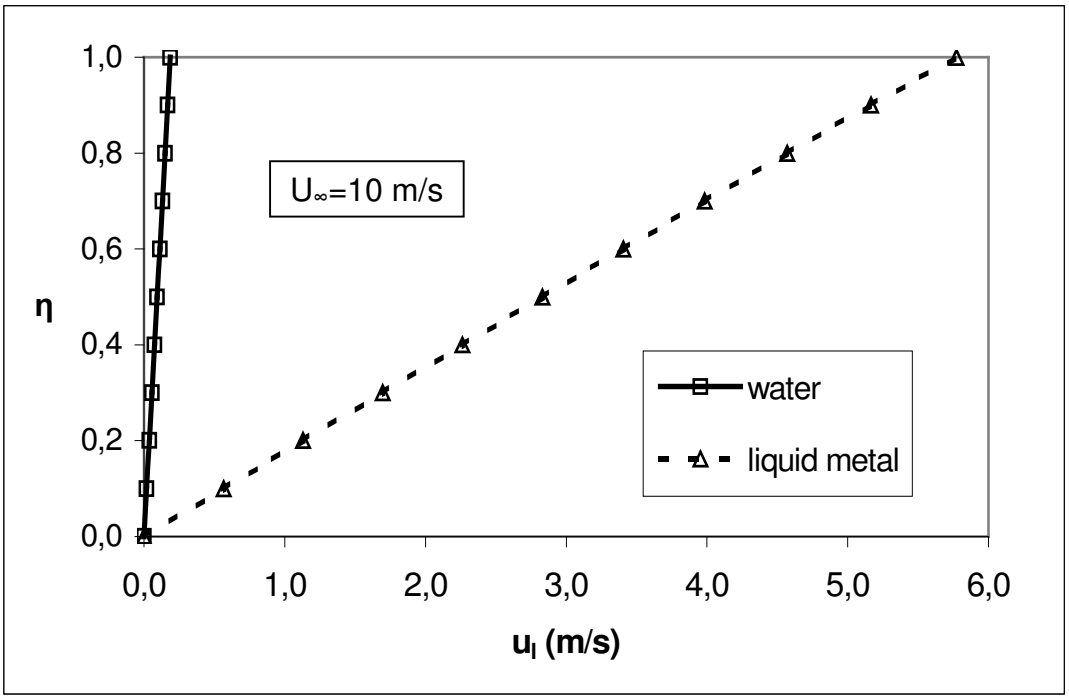

Figure 7.17. Comparison of the Velocity Profiles within the Liquid for Water and Mercury at ϕ=90°

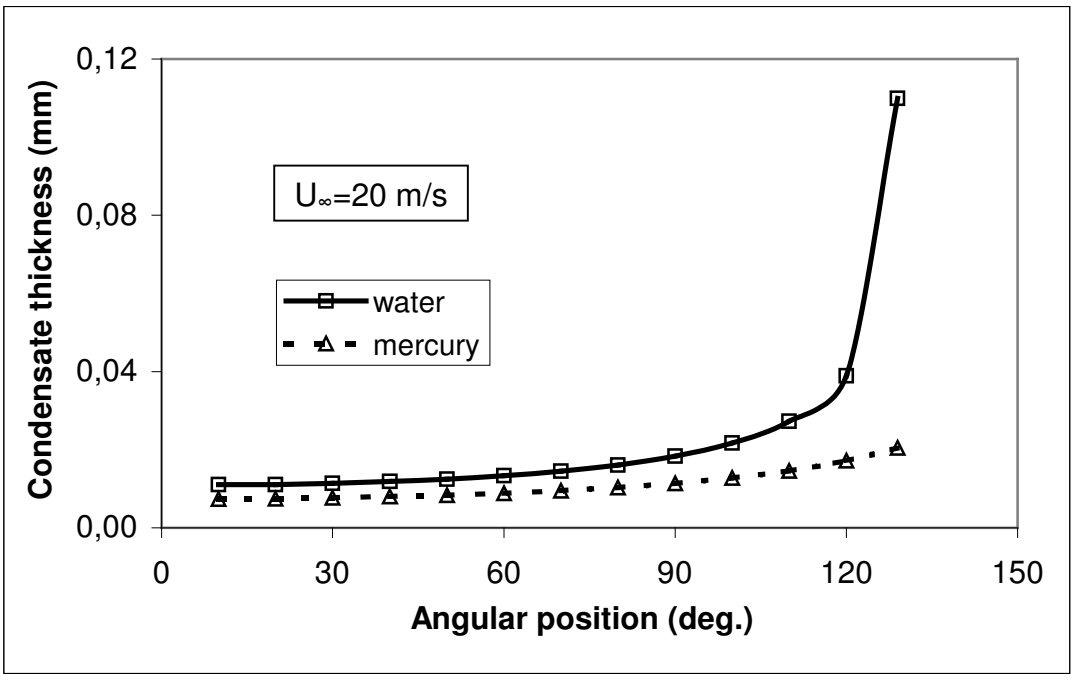

Figure 7.18. Comparison of the Condensate Thicknesses for Water and Mercury (No flow separation for Mercury)

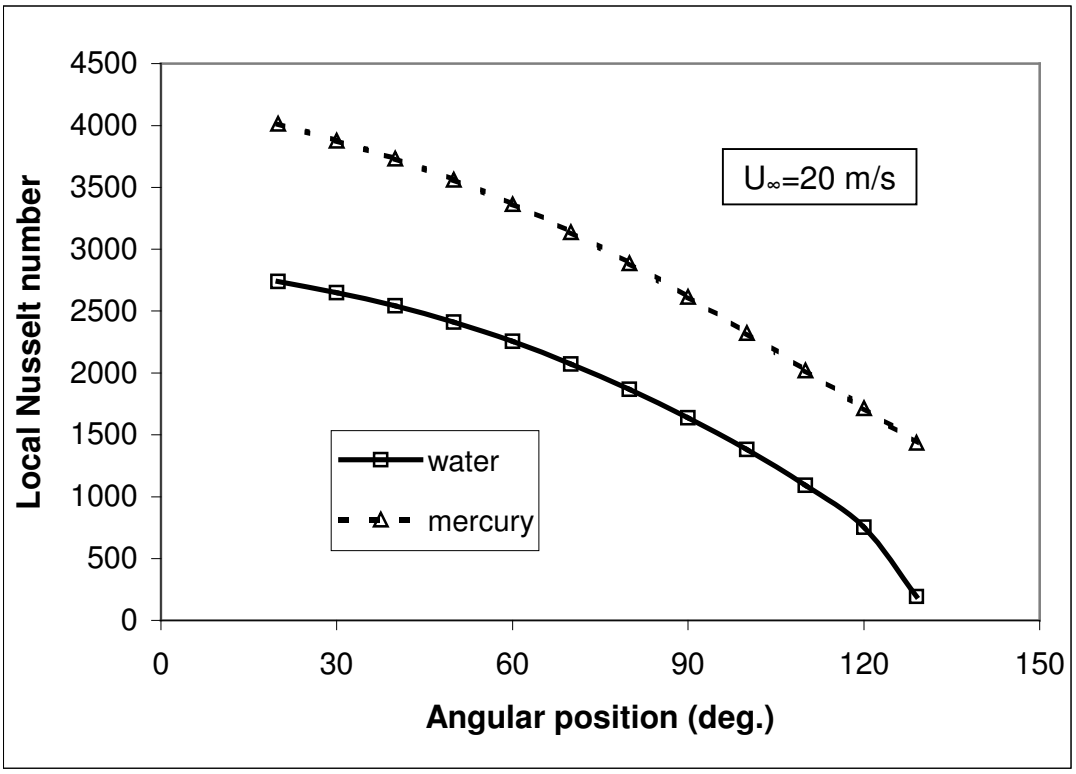

Figure 7.19. Comparison of the Local Nusselt Number for Water and Mercury

The data used in Figure 7.17. is given in Appendix B.11, and the data used in Figure 7.18. and Figure 7.19. is given in Appendix B.12.

CHAPTER 8

CONCLUSIONS AND FURTHER RECOMMENDATİONS

In this Chapter, the analytical results are discussed and further recommendations are made.

8.1. In Figure 7.1, it can be seen that the tangential vapor velocity profiles are consistent with the concepts of boundary layer theory up to 110°. After 110° the vapor boundary layer disappears and the effect of separation point appears.

8.2. In Figure 7.2., a linear scale is used to observe both condensate and vapor velocity distributions. From this figure, it can be seen that, at the interface, the effects of interfacial shear are felt, and the slope of the condensate velocity profile is less than that of the vapor velocity profile.

8.3. As shown in Figure 7.3., the tangential velocity distribution within the condensate layer is linear up to ϕ=110°. At ϕ=129°, the slope of the condensate velocity ($\partial u_l/\partial \eta$) becomes zero in the vicinity of the solid wall and flow separation occurs. From this point on, the condensate velocity distribution becomes unstable and the boundary layer equations are not valid anymore.

8.4. Figure 7.4. shows that the temperature distribution within the condensate layer is almost linear for all angular positions up to the separation point. This fact indicates that the heat transfer from the interface to the sphere wall is predominantly conduction.

8.5. A comparison of the condensate film thicknesses at various oncoming velocities, given in Figure 7.5., shows that with increasing oncoming velocity, the condensate film thickness is decreasing. This can be explained as follows; With increased oncoming velocity the velocity within the condensate also increases due to the interfacial shear. Hence, the film thickness is decreased. Figure 7.5 also indicates that, at higher oncoming velocities, the separation point moves upstream slightly. For all oncoming velocities, the condensate film thickness becomes very high near the separation point.

8.6. In Figure 7.6., the condensate film thickness with and without the pressure gradient is compared. In this Figure, it can be seen that the pressure gradient causes a small decrease in the condensate film thickness up to the end of the favorable pressure gradient region, and has the opposite effect for the adverse pressure gradient region. Additionally, the pressure gradient causes the condensate to separate, and the condensate thickness to display some unstable decreases and increases after the separation point.

8.7. In Figure 7.7., the effect of gravity and oncoming velocity on condensate film thickness is represented. From this figure, it can be seen that, at lower vapor oncoming velocities, the effect of gravity is felt more. For an oncoming velocity of 10 m/s, separation point moves from ϕ=132° to ϕ=177° as the gravity becomes 100g.

8.8. The variation of the local Nusselt number with angular position up to the separation point at various oncoming velocities is shown in Figure 7.8. According to this Figure, the local Nusselt number is decreasing

monotonically in the direction of flow. This behavior can be explained by the fact that the dominant heat transfer type in this model is conduction and the condensate film exhibits the main thermal resistance. In Figure 7.8., it can be also observed that with increasing oncoming velocity the local Nusselt number is increasing. This is also expected since the film thickness is decreasing with increasing oncoming velocity.

8.9. The effect of the pressure gradient on local Nusselt number can also be observed in Figure 7.9. It can be seen that the pressure gradient increases the heat transfer up to ϕ=90°, and decreases it from ϕ=90° up to the separation point. This behavior is expected since upstream of ϕ=90°, it is favorable pressure gradient region. Thus, including the pressure gradient results in higher velocities and consequently in lower condensate film thicknesses.

8.10. In Figure 7.10., velocity profiles within the condensate are compared for the sphere and for the cylinder. Since the potential flow velocity for the cylinder is higher, due to the interfacial shear and pressure gradient, also the condensate velocities in x-direction become higher. This velocity difference increases up to 90º, and decreases downward from this point on. This behavior can be observed better in Figure 7.11.

8.11. The separation for the cylinder takes place at 127º. In Ref.[22] the separation point for the cylinder was found to be 108 º, which is the separation point of a single-phase flow. For the case of condensation it is not realistic to have the same separation point since suction has the effect of delaying the separation point. Therefore, it can be said that the separation point found in this study is more realistic.

8.12. In Figure 7.12., the condensate film thicknesses for the downmarching flow over a sphere and over a cylinder are compared. The mass flow rate of the condensate for the flow over a sphere is proportional to

u_l, r and δ. As aforementioned, the increase of the x-velocity for the sphere becomes lower with respect to that for the cylinder up to 90º. But, the distance from the axis of symetry (r) increases. The net effect is a higher increase of the film thickness for the sphere. Downwards from 90º, the decrease of the x-velocity for the sphere becomes lower with respect to that for the cylinder. But the distance from the axis of symetry (r) increases. For this region, the net effect is also a higher increase of the film thickness for the sphere. This explains why the film thickness for the sphere reaches that for the cylinder near the separation point.

8.13. The local Nusselt number for the flow over a sphere and over a cylinder can be compared in Figure 7.13. At the beginning, the local Nusselt number is about 40% higher for the sphere. But, due to the higher increase of the film thickness with angular position, the decrease of the local Nusselt number for the sphere is higher.

8.14. In Figure 7.14., the effect of the sphere radius on the velocity profiles within the condensate can be seen. It can be seen that the radius of the sphere has almost no effect on the condensate velocities.

8.15. The effect of the sphere radius on condensate film thickness is shown in Figure 7.15. Since the downmarching distance increases with increasing sphere radius, the film thickness also increases. Because of this, the increase of the sphere radius leads also to an increase of the local Nusselt number as it can be seen from Figure 7.16. This behavior is due to the diameter term in the formulation of the local Nusselt number.

8.16. The results for Mercury show that the velocity profile for Mercury is much larger than the velocity profile of water (Figure 7.17.). This is expected, since the density of Mercury is 12 times larger than water. Also, the interfacial shear for Mercury is greater than water. Because of the higher velocities, no flow separation occurs, and the film thickness of Mercury is

lower than the film thickness of water. But, the difference is not as high as expected. This is due to the fact, that the higher conductivity of Mercury results in an increase of the heat transfer (Figure 7.19.), and due to condensation of vapor, the film thickness tends to be higher (Figure 7.18.).

8.17. The computer program written in this study may serve as a basis for experiments which include condensation of water vapor over a sphere or over a horizontal cylinder.

8.18. In further studies, the system considered in this study, can be extended to a system with staggered bundles of horizontal cylinders or spheres.

8.19. By changing the thermophysical properties, which are the input of the system, the working fluid may also be changed in advanced studies.

REFERENCES

1. Çengel, Y.A., *Heat Transfer – A Practical Approach*, International Edition,1998, McGraw-Hill

2. Kakaç, S. and Yener, Y., *Convective Heat Transfer*, 2nd Edition, 1995, CRC Press

3. Çetinkaya, C., *Analytical and Experimental Investigation of Condensation on Circular Disk under High Gravity*, 2001, M.S. Thesis

4. White, F.M., *Viscous Fluid Flow*, 2nd Edition, 1991, McGraw-Hill

5. Fox, R.W. and McDonald, A.T., *Introduction to Fluid Mechanics*, 4th Edition, 1994, John Wiley & Sons

6. Sparrow, E.M. and Gregg, J.L., A boundary-layer Treatment of Laminar Film Condensation, *Journal of Heat Transfer- Transactions of the ASME*, 1959, Vol.81C, pp.13-18

7. Sparrow, E.M., Gregg, J.L., Laminar Condensation Heat Transfer on a Horizontal Cylinder, *Journal of Heat Transfer- Transactions of the ASME*, 1959, Vol.81C, pp.291-296

8. Yang, J. W., Laminar Film Condensation on a Sphere, *Journal of Heat Transfer - Transactions of the ASME*, 1973, Vol.5C, pp.174-178

9. Koh, C.Y., Sparrow, E.M. and Harnett, J.P., The Two Phase Boundary Layer in Laminar Film Condensation, *International Journal of Heat and Mass Transfer*, 1961, Vol.2, pp.69-82

10. Chen, M.M., An Analytical Study of Laminar Film Condensation: Part1 - Flat Plates, *Journal of Heat Transfer - Transactions of the ASME*, 1961, Vol.83C, pp.48-54

11. Chen, M.M., An Analytical Study of Laminar Film Condensation: Part2 – Single and Multiple Horizontal Tubes, *Journal of Heat Transfer - Transactions of the ASME*, 1961, Vol.83C, pp.55-60

12. Koh, J.C.Y., An Integral Treatment of Two-Phase Boundary Layer in Film Condensation, *Journal of Heat Transfer - Transactions of the ASME*, 1961, Vol.83, pp.359-362

13. Churchill, S.W., Laminar Film Condensation, *International Journal of Heat and Mass Transfer*, 1986, Vol.29, No.8, pp.1219-1226

14. Taghavi, K., Effect of Surface Curvature on Laminar Film Condensation, *Journal of Heat Transfer - Transactions of the ASME*, 1988, Vol.110, pp.268-270

15. Henderson, C.L. and Marchello, J.M., Role of Surface Tension and Tube Diameter in Film Condensation on Horizontal Tubes, *AIChE Journal*, 1967, Vol.13, No.3, pp.613-614

16. Koh, J.C.Y., Film Condensation in a Forced-Convection Boundary-Layer Flow, *International Journal of Heat and Mass Transfer*, 1962, Vol.5, pp.941-954

17. Shekriladze I.G. and Gomelauri, V.I., Theoretical Study of Laminar Film Condensation of Flowing Vapor, *International Journal of Heat and MassTransfer*, 1966, Vol.9, pp.581-591

18. Denny, E.E. and Mills, A.F., Laminar Film Condensation on a Horizontal Cylinder at Normal Gravity, *Journal of Heat Transfer – Transactions of ASME*, 1969, Vol.91C, pp.495-501

19. Fujii, T., Uehara, H. and Kurata, C., Laminar Film Condensation of Flowing Vapor on a Horizontal Cylinder, *International Journal of Heat and MassTransfer*, 1972, Vol.15, pp.235-246

20. Rose, J.W., Effect of Pressure Gradient in Forced Convection Film Condensation on a Horizontal Tube, *International Journal of Heat and MassTransfer*, 1984, Vol.27, No.1, pp.39-47

21. Gaddis, E.S., Solution of Two Phase Boundary Layer Equations for Laminar Film Condensation of Vapor Flowing Perpendicular to a Horizontal Cylinder, *International Journal of Heat and MassTransfer*, 1979, Vol.22, pp.371-382

22. Karabulut, H. and Ataer, Ö.E., Numerical Analysis of Laminar Filmwise Condensation, *International Journal of Refrigeration*, 1996, Vol.19, No.2,pp.117-123

23. Memory, S.B., Adams, V.H. and Marto, P.J., Free and Forced Convection Laminar Film Condensation on Horizontal Elliptical Tubes, *International Journal of Heat and Mass Transfer*, 1997, Vol.40, No.14, pp.3395-3406

24. Schlichting, H., *Boundary Layer Theory*, 6th Edition, 1987, McGraw-Hill

APPENDIX A

THE COMPUTER PROGRAM

$\nu f := 0.31 \cdot 10^{-6}$ $\quad Tw := 365$ $\quad Ts := 375$

$kf := 0.676$ $\quad \Delta T := Ts - Tw$ $\quad R := 0.015$

$\rho f := 961.8$ $\quad hfg := 2256.7 \cdot 10^{3}$ $\quad Uin := 20$

$\rho g := 0.597$ $\quad \mu f := 0.298 \cdot 10^{-3}$ $\quad g := 9.81$

$\nu g := 0.02 \cdot 10^{-3}$ $\quad \mu g := 1.255 \cdot 10^{-5}$ $\quad Cp := 4210.7$

Result :=

$\delta_1 \leftarrow \left(\frac{\nu f \cdot 3 \cdot kf \cdot \Delta T \cdot R}{2 \cdot g \cdot \rho f \cdot hfg} \right)^{\frac{1}{4}}$

$\Delta y \leftarrow 1 \cdot 10^{-5}$

$\Delta x \leftarrow 2.6 \cdot 10^{-4}$

$\Delta \eta \leftarrow 1 \cdot 10^{-1}$

$n \leftarrow \frac{1}{\Delta \eta}$

$x \leftarrow 0$

$L \leftarrow \frac{0.00025}{\Delta y}$

$m \leftarrow \frac{0.047}{\Delta x}$

for $i \in 1..m$

$u_{i,0} \leftarrow 0$

$v_{i,0} \leftarrow 0$

$T_{i,0} \leftarrow 365$

$x \leftarrow i \cdot \Delta x$

$T_{i,n} \leftarrow 375$

$ro_i \leftarrow R \cdot \sin\left(\frac{x}{R}\right)$

$U\psi_i \leftarrow \frac{3}{2} \cdot Uin \cdot \sin\left(\frac{x}{R}\right)$

for $j \in 1..n$

$\eta \leftarrow j \cdot \Delta\eta$

$u_{1,j} \leftarrow \frac{g \cdot (\delta_1)^2 \cdot \Delta x}{\nu f \cdot R} \cdot \left[\eta - \frac{(\eta)^2}{2}\right]$

$v_{1,j} \leftarrow \frac{g \cdot (\delta_1)^3}{\nu f \cdot R} \cdot \left[\frac{(\eta)^3}{6} - \frac{(\eta)^2}{2}\right] - \frac{u_{1,j} \cdot \delta_1 \cdot \eta}{\Delta x}$

for $j \in 1..n-1$

$\eta \leftarrow j \cdot \Delta\eta$

$T_{1,j} \leftarrow \left[(Ts - Tw) \cdot \eta + Tw\right]$

for $i \in 1..m-1$

for $k \in 0..L$

$UV_{1,k} \leftarrow u_{1,n}$

$VV_{1,k} \leftarrow v_{1,n}$

for $j \in 1..n-1$

$A \leftarrow \frac{\mu g \cdot \delta_i \cdot \Delta\eta}{\mu f \cdot \Delta y}$

$\alpha_j \leftarrow \frac{\nu f \cdot \Delta x}{(\delta_i)^2 \cdot u_{i,j} \cdot \Delta\eta^2}$

$C_j \leftarrow \frac{\rho g}{\rho f} \cdot \frac{(U\psi_{i+1})^2 - (U\psi_i)^2}{2 \cdot u_{i,j}} - \frac{\Delta x \cdot v_{i,j}}{\delta_i \cdot u_{i,j}} \cdot \frac{u_{i,j+1} - u_{i,j-1}}{2 \cdot \Delta\eta} + u_{i,j} + g \cdot \sin\left(\frac{x}{R}\right) \cdot \frac{\Delta x}{u_{i,j}}$

for $k \in 1..L-1$

$\gamma_k \leftarrow \frac{\nu g \cdot \Delta x}{UV_{i,k} \cdot \Delta y^2}$

$E_k \leftarrow \frac{(U\psi_{i+1})^2 - (U\psi_i)^2}{2 \cdot UV_{i,k}} - \frac{\Delta x \cdot VV_{i,k}}{UV_{i,k}} \cdot \frac{UV_{i,k+1} - UV_{i,k-1}}{2 \cdot \Delta y} + UV_{i,k}$

$P_1 \leftarrow \frac{\alpha_1}{1 + 2 \cdot \alpha_1}$

$Q_1 \leftarrow \frac{C_1}{1 + 2 \cdot \alpha_1}$

for $j \in 3..n$

$$P_{j-1} \leftarrow \frac{\alpha_{j-1}}{1 + 2 \cdot \alpha_{j-1} - \alpha_{j-1} \cdot P_{j-2}}$$

$$Q_{j-1} \leftarrow \frac{\alpha_{j-1} \cdot Q_{j-2} + C_{j-1}}{1 + 2 \cdot \alpha_{j-1} - \alpha_{j-1} \cdot P_{j-2}}$$

$$PV_0 \leftarrow \frac{A}{1 + A - P_{n-1}}$$

$$QV_0 \leftarrow \frac{Q_{n-1}}{1 + A - P_{n-1}}$$

for $k \in 2..L$

$$PV_{k-1} \leftarrow \frac{\gamma_{k-1}}{1 + 2 \cdot \gamma_{k-1} - \gamma_{k-1} \cdot PV_{k-2}}$$

$$QV_{k-1} \leftarrow \frac{\gamma_{k-1} \cdot QV_{k-2} + E_{k-1}}{1 + 2 \cdot \gamma_{k-1} - \gamma_{k-1} \cdot PV_{k-2}}$$

$$UV_{i+1,L} \leftarrow U\psi_{i+1}$$

for $k \in L..1$

$$UV_{i+1,k-1} \leftarrow PV_{k-1} \cdot UV_{i+1,k} + QV_{k-1}$$

$$u_{i+1,n} \leftarrow UV_{i+1,0}$$

for $j \in n..2$

$$u_{i+1,j-1} \leftarrow P_{j-1} \cdot u_{i+1,j} + Q_{j-1}$$

$$sumx1 \leftarrow 0$$

$$sumx2 \leftarrow 0$$

for $j \in 0..n-1$

$$sumx1 \leftarrow sumx1 + u_{i+1,j} + u_{i+1,j+1}$$

$$sumx2 \leftarrow sumx2 + u_{i,j} + u_{i,j+1}$$

$$\delta_{i+1} \leftarrow \frac{\dfrac{2 \cdot \Delta x \cdot kf \cdot ro_i \cdot \left(T_{i,1} - T_{i,0}\right)}{hfg \cdot \rho f \cdot \delta_i \cdot \Delta\eta^2} + ro_{i+1} \cdot \delta_i \cdot sumx1}{ro_{i+1} \cdot sumx1 + ro_{i+1} \cdot (sumx1 - sumx2) + \left(ro_{i+1} - ro_i\right) \cdot sumx1}$$

for $j \in 1..n-1$

$$\beta_j \leftarrow \frac{kf \cdot \Delta x}{\rho f \cdot Cp \cdot \left(\delta_{i+1}\right)^2 \cdot \Delta\eta^2}$$

$$F_j \leftarrow T_{i,j} - \frac{\Delta x \cdot v_{i,j}}{\delta_i \cdot u_{i,j}} \cdot \frac{\left(T_{i,j+1} - T_{i,j}\right)}{\Delta\eta}$$

for $i \in 1..m-1$

$PT_1 \leftarrow \dfrac{\beta_1}{1+2\cdot\beta_1}$

$QT_1 \leftarrow \dfrac{\beta_1\cdot T_{i,0}+F_1}{1+2\cdot\beta_1}$

for $j \in 3..n$

$PT_{j-1} \leftarrow \dfrac{\beta_{j-1}}{1+2\cdot\beta_{j-1}-\beta_{j-1}\cdot PT_{j-2}}$

$QT_{j-1} \leftarrow \dfrac{\beta_{j-1}\cdot QT_{j-2}+F_{j-1}}{1+2\cdot\beta_{j-1}-\beta_{j-1}\cdot PT_{j-2}}$

for $j \in n..2$

$T_{i+1,j-1} \leftarrow PT_{j-1}\cdot T_{i+1,j}+QT_{j-1}$

for $j \in 1..n$

$v_{i+1,j} \leftarrow v_{i+1,j-1}-\dfrac{\Delta\eta\cdot\delta_{i+1}}{2\cdot\Delta x\cdot ro_{i+1}}\cdot\left[ro_{i+1}\cdot\left(u_{i+1,j}-u_{i+1,j-1}\right)-ro_i\cdot\left(u_{i,j}-u_{i,j-1}\right)\right]$

$VV_{i+1,0} \leftarrow UV_{i+1,0}\cdot\left(\dfrac{\delta_{i+1}-\delta_i}{\Delta x}\right)-\dfrac{kf\cdot\left(T_{i+1,1}-T_{i+1,0}\right)}{hfg\cdot\rho g\cdot\delta_{i+1}\cdot\Delta\eta}$

for $k \in 1..L$

$VV_{i+1,k} \leftarrow VV_{i+1,k-1}-\dfrac{\Delta y}{2\cdot\Delta x\cdot ro_{i+1}}\cdot\left[ro_{i+1}\cdot\left(UV_{i+1,k}-UV_{i+1,k-1}\right)-ro_i\cdot\left(UV_{i,k}-UV_{i,k-1}\right)\right]$

$h_i \leftarrow \dfrac{kf\cdot\left(T_{i,1}-T_{i,0}\right)}{\Delta\eta\cdot\delta_i\cdot(Ts-Tw)}$

$Nu_i \leftarrow \dfrac{2\cdot R\cdot h_i}{kf}$

for $j \in 1..n$

$\eta \leftarrow j\cdot\Delta\eta$

$Y_{i+1,j} \leftarrow \eta\cdot\delta_{i+1}$

Nu

APPENDIX B

RESULTS OF NUMERICAL ANALYSIS

B.1 Tangential Velocity Distribution for Condensate and Vapor

The tangential velocity distribution for condensate and vapor with respect to y are given in Table B.1. In the table; x is in degree, y is in mm and u is in m/s.

Table B.1 Tangential Velocity Distribution for Condensate and Vapor

Condensate											
x → 30		60		90		110		120		129	
y	u	y	u	y	u	y	u	y	u	y	u
0,000	0,000	0,000	0,000	0,000	0,000	0,000	0,000	0,000	0,000	0,000	0,000
0,001	0,019	0,001	0,033	0,002	0,037	0,003	0,032	0,004	0,024	0,011	0,003
0,002	0,038	0,003	0,066	0,004	0,074	0,005	0,063	0,008	0,049	0,022	0,009
0,003	0,057	0,004	0,099	0,005	0,111	0,008	0,095	0,012	0,075	0,033	0,019
0,005	0,076	0,005	0,132	0,007	0,148	0,011	0,128	0,016	0,101	0,044	0,032
0,006	0,095	0,007	0,165	0,009	0,185	0,014	0,160	0,019	0,128	0,055	0,049
0,007	0,113	0,008	0,197	0,011	0,222	0,016	0,193	0,023	0,155	0,066	0,068
0,008	0,132	0,009	0,230	0,013	0,259	0,019	0,226	0,027	0,183	0,077	0,089
0,009	0,151	0,011	0,262	0,015	0,296	0,022	0,259	0,031	0,212	0,088	0,113
0,010	0,169	0,012	0,295	0,016	0,333	0,025	0,292	0,035	0,241	0,099	0,138
0,011	0,188	0,013	0,327	0,018	0,370	0,027	0,326	0,039	0,270	0,110	0,164

Table B.1 Continued

Vapor											
x → 30		60		90		110		120		129	
y	u	y	u	y	u	y	u	y	u	y	u
0,011	0,188	0,013	0,327	0,018	0,370	0,027	0,326	0,039	0,270	0,110	0,164
0,021	3,654	0,023	5,600	0,028	4,934	0,037	3,236	0,049	2,150	0,120	1,010
0,031	6,338	0,033	9,848	0,038	8,888	0,047	5,960	0,059	4,022	0,130	1,975
0,041	8,405	0,043	13,253	0,048	12,304	0,057	8,500	0,069	5,876	0,140	3,048
0,051	9,989	0,053	15,971	0,058	15,240	0,067	10,859	0,079	7,699	0,150	4,216
0,061	11,200	0,063	18,130	0,068	17,752	0,077	13,033	0,089	9,475	0,160	5,460
0,071	12,121	0,073	19,838	0,078	19,886	0,087	15,022	0,099	11,187	0,170	6,760
0,081	12,821	0,083	21,185	0,088	21,689	0,097	16,826	0,109	12,819	0,180	8,093
0,091	13,352	0,093	22,242	0,098	23,203	0,107	18,448	0,119	14,360	0,190	9,437
0,101	13,753	0,103	23,070	0,108	24,467	0,117	19,894	0,129	15,798	0,200	10,771
0,111	14,056	0,113	23,717	0,118	25,516	0,127	21,173	0,139	17,127	0,210	12,074
0,121	14,284	0,123	24,219	0,128	26,383	0,137	22,295	0,149	18,342	0,220	13,330
0,131	14,455	0,133	24,610	0,138	27,095	0,147	23,273	0,159	19,443	0,230	14,524
0,141	14,583	0,143	24,912	0,148	27,678	0,157	24,118	0,169	20,432	0,240	15,648
0,151	14,678	0,153	25,146	0,158	28,153	0,167	24,846	0,179	21,314	0,250	16,693
0,161	14,749	0,163	25,325	0,168	28,540	0,177	25,468	0,189	22,095	0,260	17,657
0,171	14,801	0,173	25,464	0,178	28,853	0,187	25,998	0,199	22,783	0,270	18,539
0,181	14,838	0,183	25,570	0,188	29,106	0,197	26,449	0,209	23,386	0,280	19,341
0,191	14,865	0,193	25,651	0,198	29,311	0,207	26,831	0,219	23,913	0,290	20,067
0,201	14,884	0,203	25,713	0,208	29,477	0,217	27,154	0,229	24,373	0,300	20,722
0,211	14,896	0,213	25,760	0,218	29,611	0,227	27,428	0,239	24,775	0,310	21,313
0,221	14,904	0,223	25,796	0,228	29,720	0,237	27,662	0,249	25,128	0,320	21,848
0,231	14,908	0,233	25,823	0,238	29,809	0,247	27,862	0,259	25,439	0,330	22,336
0,241	14,909	0,243	25,844	0,248	29,883	0,257	28,036	0,269	25,715	0,340	22,785
0,251	14,909	0,253	25,860	0,258	29,945	0,267	28,188	0,279	25,965	0,350	23,204
0,261	14,906	0,263	25,872	0,268	29,998	0,277	28,324	0,289	26,194	0,360	23,604

B.2 Variation of the Condensate Thickness with Vapor Oncoming Velocity

The variation of the condensate film thickness with angular position for U=10,20 and 60 m/s is given in Table B.2.

Table B.2. Variation of the Condensate Thickness (mm) with Vapor Oncoming Velocity (Up to flow separation)

x (degree)	U_∞=10 m/s	U_∞=20 m/s	U_∞=60 m/s
10	0,015	0,011	0,007
20	0,016	0,011	0,006
30	0,016	0,011	0,007
40	0,017	0,012	0,007
50	0,018	0,012	0,007
60	0,019	0,013	0,008
70	0,020	0,014	0,008
80	0,023	0,016	0,009
90	0,026	0,018	0,011
100	0,030	0,022	0,013
110	0,038	0,027	0,016
120	0,051	0,039	0,022
125	0,065	0,053	0,031
126	0,069	0,059	0,034
127	0,074	0,067	0,038
128	0,080	0,080	0,046
129	0,088	0,110	0,063
130	0,099		
131	0,117		
132	0,155		

B.3 Variation of the Condensate Thickness with Pressure Gradient

The variation of the condensate film thickness with angular position, including and neglecting the pressure gradient, is given in Table B.3. The vapor oncoming velocity was taken as 20 m/s.

Table B.3. Variation of the Condensate Thickness (mm) with Pressure Gradient (Up to flow separation)

x (degree)	With Pressure Gradient	Without Pressure Gradient
10	0,011	0,015
20	0,011	0,015
30	0,011	0,015
40	0,012	0,016
50	0,012	0,016
60	0,013	0,017
70	0,014	0,017
80	0,016	0,018
90	0,018	0,019
100	0,022	0,021
110	0,027	0,023
120	0,039	0,025
121	0,041	0,026
122	0,043	0,026
123	0,046	0,026
124	0,049	0,027
125	0,053	0,027
126	0,059	0,027
127	0,067	0,028
128	0,080	0,028
129	0,110	0,029

B.4 Variation of the Local Nusselt Number with Vapor Oncoming Velocity

The variation of the local Nusselt number with angular position for U=10,20 and 60 m/s is given in Table B.4.

Table B.4. Variation of the Local Nusselt Number with Vapor Oncoming Velocity (Up to flow separation)

x (degree)	U_∞=10 m/s	U_∞=20 m/s	U_∞=60 m/s
10	1987	2750	4155
20	1945	2733	4628
30	1882	2649	4546
40	1804	2541	4375
50	1711	2410	4154
60	1601	2254	3888
70	1473	2073	3579
80	1328	1868	3226
90	1167	1637	2831
100	988	1381	2391
110	791	1093	1900
120	567	753	1323
125	434	528	947
129	298	193	393
130	253		
131	197		
132	118		

B.5 Variation of the Local Nusselt Number with Pressure Gradient

The variation of the local Nusselt number with angular position, including and neglecting the pressure gradient, is given in Table B.5. The vapor oncoming velocity was taken as 20 m/s.

Table B.5. Variation of the Local Nusselt Number with Pressure Gradient
(Up to flow separation with pressure gradient)

x (degree)	With Pressure Gradient	Without Pressure Gradient
10	2750	2023
20	2733	1995
30	2649	1954
40	2541	1909
50	2410	1857
60	2254	1796
70	2073	1726
80	1868	1644
90	1637	1550
100	1381	1443
110	1093	1322
120	753	1185
125	528	1111
126	470	1096
127	402	1080
128	316	1064
129	193	1049

B.6 Comparison of the Condensate Velocities for the Sphere and Cylinder

The results for the variation of the velocities within the condensate with respect to the dimensionless film thickness, η, for the sphere and for the cylinder are given in Table B.6. The vapor oncoming velocity was taken as 20 m/s, and the results are given for the angular positions; 60°, 90° and 120° respectively.

Table B.6. Comparison of the Condensate Velocities for the Sphere and Cylinder (x in degree, u in m/s)

	x → 60		90		120	
η	Sphere	Cylinder	Sphere	Cylinder	Sphere	Cylinder
0	0,000	0,000	0,000	0,000	0,000	0,000
0,1	0,033	0,049	0,037	0,052	0,024	0,028
0,2	0,066	0,098	0,074	0,104	0,049	0,057
0,3	0,099	0,147	0,111	0,156	0,075	0,088
0,4	0,132	0,195	0,148	0,208	0,101	0,120
0,5	0,165	0,243	0,185	0,260	0,128	0,153
0,6	0,197	0,291	0,222	0,312	0,155	0,187
0,7	0,230	0,339	0,259	0,364	0,183	0,222
0,8	0,262	0,386	0,296	0,416	0,212	0,258
0,9	0,295	0,434	0,333	0,467	0,241	0,294
1	0,327	0,481	0,370	0,519	0,270	0,332

B.7 Comparison of the Condensate Thickness and Local Nusselt Number for the Sphere and Cylinder

The results for the variation of the condensate thickness and local Nusselt number with angular position for the sphere and for the cylinder are given in Table B.7. The vapor oncoming velocity was taken as 20 m/s.

Table B.7. Comparison of the Condensate Thickness and Local Nusselt Number for the Sphere and Cylinder (Up to flow separation)

	Condensate Thickness (mm)		Nusselt Number	
X	Cylinder	Sphere	Cylinder	Sphere
10	0,017	0,011	1800	2750
20	0,015	0,011	2040	2737
30	0,014	0,011	2118	2649
40	0,014	0,012	2102	2541
50	0,015	0,012	2041	2410
60	0,015	0,013	1948	2254
70	0,016	0,014	1828	2073
80	0,018	0,016	1682	1868
90	0,020	0,018	1511	1637
100	0,023	0,022	1310	1381
110	0,028	0,027	1069	1093
120	0,039	0,039	741	753
121	0,042	0,041	697	713
122	0,044	0,043	648	672
123	0,048	0,046	594	627
124	0,053	0,049	531	580
125	0,060	0,053	454	528
126	0,073	0,059	351	470
127	0,109	0,067	186	402
128		0,080		316
129		0,110		193

B.8 Effect of Sphere Radius on Condensate Velocity

The results for the variation of the velocities within the condensate with respect to the dimensionless film thickness (η) for r_0=15 mm and r_0=30 mm are given in Table B.8. The vapor oncoming velocity was taken as 20 m/s, and the results are given for the angular positions; 60°, 90° and 120° respectively.

Table B.8. Comparison of the Condensate Velocities for r_0=15mm and r_0=30mm (x in degree, u in m/s)

	x→ 60		90		120	
η	Sphere	Cylinder	Sphere	Cylinder	Sphere	Cylinder
0	0,000	0.000	0,000	0.000	0,000	0.000
0,1	0,033	0.033	0,037	0.037	0,024	0.025
0,2	0,066	0.066	0,074	0.074	0,049	0.050
0,3	0,099	0.099	0,111	0.112	0,075	0.076
0,4	0,132	0.132	0,148	0.149	0,101	0.103
0,5	0,165	0.165	0,185	0.186	0,128	0.130
0,6	0,197	0.198	0,222	0.223	0,155	0.158
0,7	0,230	0.230	0,259	0.260	0,183	0.187
0,8	0,262	0.263	0,296	0.297	0,212	0.216
0,9	0,295	0.295	0,333	0.335	0,241	0.245
1	0,327	0.328	0,370	0.372	0,270	0.275

B.9 Effect of Sphere Radius on Condensate Thickness and Local Nusselt Number

The results for the variation of the condensate thickness and local Nusselt number with angular position for r_0=15 mm and r_0=30 mm are given in Table B.9. The vapor oncoming velocity was taken as 20 m/s.

Table B.9. Comparison of the Condensate Thickness and Local Nusselt Number for r_0=15mm and r_0=30mm (Up to flow separation)

	Condensate Thickness (mm)		Nusselt Number	
x	r_0=15 mm	r_0=30 mm	r_0=15 mm	r_0=30 mm
10	0,011	0,015	2750	3925
20	0,011	0,016	2737	3884
30	0,011	0,016	2649	3752
40	0,012	0,017	2541	3599
50	0,012	0,018	2410	3413
60	0,013	0,019	2254	3192
70	0,014	0,020	2073	2936
80	0,016	0,023	1868	2646
90	0,018	0,026	1637	2321
100	0,022	0,031	1381	1960
110	0,027	0,038	1093	1557
120	0,039	0,054	753	1088
121	0,041	0,057	713	1034
122	0,043	0,060	672	978
123	0,046	0,063	627	918
124	0,049	0,067	580	856
125	0,053	0,072	528	788
126	0,059	0,078	470	714
127	0,067	0,087	402	631
128	0,080	0,099	316	531
129	0,110	0,121	193	403

B.10 Thermophysical Properties of Mercury

Table B.10. Thermophysical Properties of Mercury

	Chemical formula: Hg Molecular weight: 200.51 Normal boiling point: 630.1 K Melting point: 324.32 K						Critical temperature: 1763.2 K Critical pressure: 151000 kPa Critical density: 5500 kg/m^3			
T_{sat} (K)	**630.1**	**650**	**700**	**750**	**800**	**850**	**900**	**950**	**1000**	**1050**
p_{sat} (kPa)	**101.3**	**145**	**316**	**620**	**1120**	**1880**	**2990**	**4530**	**6580**	**9230**
ρ_l (kg/m^3)	12737	12688	12567	12444	12318	12190	12059	11927	11791	11650
ρ_g (kg/m^3)	3.91	5.37	10.9	20.1	34.2	54.6	82.7	119.9	167.7	227.3
h_l (kJ/kg)	91.8	94.5	101.3	108.2	115.2	122.3	129.5	136.9	144.4	153.8
h_g (kJ/kg)	386.7	388.7	393.6	398.4	403.0	407.4	411.6	415.5	419.1	423.0
$\Delta h_{g,l}$ (kJ/kg)	294.9	294.2	292.3	290.2	287.8	285.1	282.1	278.6	274.7	269.2
$c_{p,l}$ [kJ/(kg · K)]	0.136	0.136	0.137	0.138	0.140	0.142	0.144	0.146	0.149	0.153
$c_{p,g}$ [kJ/(kg · K)]	0.104	0.104	0.105	0.106	0.107	0.108	0.109	0.111	0.113	0.116
η_l [(μN · s)/m^2]	884	870	841	816	794	776	760	746	736	723
η_g [(μN · s)/m^2]	61.7	63.5	68.6	73.5	78.4	83.5	88.4	93.2	98.0	103.0
λ_l [(mW/m^2)/(K/m)]	121.90	123.60	128.00	131.90	135.10	137.80	141.80	144.50	146.90	147.90
λ_g [(mW/m^2)/(K/m)]	10.4	10.8	11.7	12.6	13.5	14.4	15.3	16.2	17.2	18.1
Pr_l	0.987	0.957	0.900	0.854	0.823	0.800	0.772	0.754	0.744	0.748
Pr_g	0.617	0.612	0.616	0.618	0.621	0.626	0.630	0.637	0.644	0.660
σ [(m · N)/m]										
$\beta_{e,l}$ (kK^{-1})	0.194	0.193	0.195	0.203	0.212	0.221	0.230	0.241	0.253	0.269

B.11 Comparison of the Condensate Velocities for Mercury and Water

The results for the variation of the velocities within the condensate with respect to the dimensionless film thickness (η) for Mercury and water are given in Table B.11. The vapor oncoming velocity was taken as 10 m/s, and the results are given for an angular position of 90°.

Table B.11. Comparison of the Condensate Velocities for Mercury and Water at ϕ=90° (u in m/s)

η	Water	Mercury
0,0	0,000	0,000
0,1	0,019	0,565
0,2	0,038	1,130
0,3	0,056	1,696
0,4	0,075	2,263
0,5	0,094	2,832
0,6	0,113	3,405
0,7	0,131	3,983
0,8	0,150	4,569
0,9	0,169	5,165
1	0,188	5,774

B.12 Comparison of the Condensate Thickness and Local Nusselt Number for Mercury and Water

The results for the variation of the condensate thickness and local Nusselt number with angular position for Mercury and water are given in Table B.12. The vapor oncoming velocity was taken as 20 m/s.

Table B.12. Comparison of the Condensate Thickness and Local Nusselt Number for Mercury and Water (Up to flow separation of water)

	Condensate Thickness (mm)		Nusselt Number	
x	Water	Mercury	Water	Mercury
10	0,011	0,007		
20	0,011	0,007	2737	4014
30	0,011	0,008	2649	3878
40	0,012	0,008	2541	3734
50	0,012	0,008	2410	3563
60	0,013	0,009	2254	3364
70	0,014	0,009	2073	3137
80	0,016	0,010	1868	2885
90	0,018	0,011	1637	2613
100	0,022	0,013	1381	2323
110	0,027	0,015	1093	2021
120	0,039	0,017	753	1714
129	0,110	0,020	193	1437